



OPEN

The effect of NMDA-R antagonist, MK-801, on neuronal mismatch along the rat auditory thalamocortical pathway

Gloria G. Parras^{1,2}, Catalina Valdés-Baizaba^{1,2}, Lauren Harms^{4,5,6}, Patricia T. Michie^{3,4,5} & Manuel S. Malmierca^{1,2,7}✉

Efficient sensory processing requires that the brain maximize its response to unexpected stimuli, while suppressing responsivity to expected events. Mismatch negativity (MMN) is an auditory event-related potential that occurs when a regular pattern is interrupted by an event that violates the expected properties of the pattern. According to the predictive coding framework there are two mechanisms underlying the MMN: repetition suppression and prediction error. MMN has been found to be reduced in individuals with schizophrenia, an effect believed to be underpinned by glutamate *N*-methyl-*D*-aspartate receptor (NMDA-R) dysfunction. In the current study, we aimed to test how the NMDA-R antagonist, MK-801 in the anaesthetized rat, affected repetition suppression and prediction error processes along the auditory thalamocortical pathway. We found that low-dose systemic administration of MK-801 differentially affect thalamocortical responses, namely, increasing thalamic repetition suppression and cortical prediction error. Results demonstrate an enhancement of neuronal mismatch, also confirmed by large scale-responses. Furthermore, MK-801 produces faster and stronger dynamics of adaptation along the thalamocortical hierarchy. Clearly more research is required to understand how NMDA-R antagonism and dosage affects processes contributing to MMN. Nonetheless, because a low dose of an NMDA-R antagonist increased neuronal mismatch, the outcome has implications for schizophrenia treatment.

Abbreviations

NMDA-R	<i>N</i> -Methyl- <i>D</i> -aspartate receptor
MMN	Mismatch negativity
ERP	Event-related potentials
AC	Auditory cortex
MGB	Medial geniculate body
L	Lemniscal
NL	Non-lemniscal
DEV	Deviant
STD	Standard
CAS	Cascade
MSC	Many-standard
FRA	Frequency–response area
PSTH	Peri-stimulus time histogram
SFR	Spontaneous firing rate

¹Cognitive and Auditory Neuroscience Laboratory, Institute of Neuroscience of Castilla y León (INCYL), Salamanca, Spain. ²The Salamanca Institute for Biomedical Research (IBSAL), Salamanca, Spain. ³School of Psychology, University of Newcastle, Callaghan, NSW, Australia. ⁴Priority Centre for Brain and Mental Health Research, Callaghan, NSW, Australia. ⁵Hunter Medical Research Institute, Newcastle, NSW, Australia. ⁶School of Biomedical Sciences and Pharmacy, University of Newcastle, Callaghan, NSW, Australia. ⁷Department of Cell Biology and Pathology, Faculty of Medicine, University of Salamanca, Salamanca, Spain. ✉email: msm@usal.es

SDF	Spike density function
iMM	Neural mismatch index
iPE	Prediction error index
iRS	Repetition suppression index
LFP	Local field potential
TRN	Thalamic reticular nucleus

The detection of changes in the sensory environment is an important function of the nervous system. When the EEG is recorded during an *oddball* sequence, in which an unexpected discriminably different stimulus (deviant, DEV) interrupts a train of regular stimuli (standards, STD), the EEG signal exhibits a negative event-related potential (ERP) peak referred to as mismatch negativity (MMN)¹. MMN is a pre-attentive signal commonly quantified as the difference between the amplitude of the DEV- and STD ERPs, and relies particularly on intact right lateral temporal and frontal top-down feedback circuits².

The predictive coding framework has emerged as an appealing model of MMN³ and of how sensory information is processed. According to this model, the brain constantly generates top-down predictions that are compared with sensory bottom-up signals. Neural responses to stimuli that match predictions are suppressed, whereas unexpected stimuli discrepant with the prediction generate an enhanced error signal^{4–6}. There are two mechanisms underlying the MMN difference signal according to the predictive coding model. First, MMN could reflect *repetition suppression*. When the same stimulus is repeatedly presented, neuronal populations sensitive to that stimulus undergo adaptation and neural responses decrease⁷. MMN could also reflect a process of *prediction error*, where the sensory memory of regular stimuli that establishes a predictive model is violated upon the presentation of an unexpected DEV stimulus. This violation results in an enhanced neural response, allowing detection of the environmental change and an update of the predictive model. Prediction error has been observed in human and rodent surface recordings when suitable control conditions have been included in the design of sound sequences^{8–11}. Essentially, there is evidence in both humans and rodents that MMN receives contributions from both prediction error and repetition suppression at various levels of the auditory system^{11, 12}.

MMN reduction occurs in healthy volunteers administered an NMDA-R antagonist¹³ and has been reported in over 100 separate reports in individuals diagnosed with schizophrenia¹⁴, leading to assertions that MMN indexes the functional state of NMDA-R neurotransmission¹⁵. The schizophrenia findings fit with current views that NMDA-R hypofunction contributes to the neuropathology of the disorder^{16, 17}. Mismatch-like responses in animal models have shown a similar sensitivity to NMDA-R antagonism^{17–21}, though it has also been reported that low doses of NMDA-R antagonist can increase rat mismatch responses²². MK-801 is a NMDA-R antagonist that has been widely used²³. Interestingly, the use of low doses of MK-801 have physiological effects as previously demonstrated in different systems other than the auditory system, such as the acquisition of associative learning in the classical conditioning of eyeblink responses^{24–26}. It is generally accepted that NMDA-R antagonists reduce MMN¹⁴. However, recent data has demonstrated that the link between NMDA-R and MMN is not as clear as previously thought²⁷.

Our primary interest here is to test whether MK-801 differentially affects repetition suppression and prediction error at the single-unit level at both the thalamic level and cortex. While previous studies have demonstrated that MMN-like responses in rodents are altered by NMDA-R antagonists^{21, 28–30}, only one report has examined the impact on prediction error component of the MMN in surface recordings²². There are no published data on the effects of NMDA-R antagonists on repetition suppression. There are no reports that have examined the impact of NMDA-R antagonists on single-unit activity and local field potential recordings from the thalamus and auditory cortex. More importantly, because the thalamus and cortex have different microcircuits that involve excitatory and inhibitory neurons and different bottom-up and top-down interconnections³¹, it is likely that the effects of MK-801 will not be the same at these two levels of the auditory hierarchy.

Thus, it is unknown (i) whether there are differential effects of NMDA-R antagonism on prediction error as opposed to repetition suppression at the single unit or local field potential level, and (ii) the regional specificity of where effects of NMDA-R antagonists occur: in the lemniscal (L) vs. non-lemniscal (NL) auditory areas, or the thalamus vs. cortex. Therefore, we used an acute exposure to a systemic low dose of MK-801 to examine the impact of NMDA-R antagonism on individual responses of lemniscal and non-lemniscal thalamocortical neurons while auditory oddball, many standards and cascade control sequences were presented (Fig. 1a,b). Systemic administration of the drug was chosen in order to mimic as closely as possible human research that found that infusion of ketamine, an NMDA-R antagonist, via the antecubital vein reduced MMN¹³. Importantly, the dose of 0.1 mg/kg MK-801 was chosen because it is sufficient to induce behavioral changes and changes to NMDA-R subunit expression in young adult female rats^{32, 33}, similar to those used in this study. This is also the dose in which peak locomotor activation is seen in female rats³⁴. Male animals require a higher MK-801 dose (0.3 mg/kg) to induce behavioral changes³³. This design allowed us to delineate effects on repetition suppression vs. prediction error (Fig. 1c)^{11, 19, 35, 36}. Unexpectedly, we found that MK-801 *increased* repetition suppression in the thalamic regions, enhanced prediction error in the cortex, and *increased* neuronal mismatch at both locations.

Material and methods

Experiments were performed on 48 (control = 25; MK-801 = 23) adult, female Long-Evans rats with body weights between 200 and 250 g (aged 9 to 15 weeks). All experimental procedures were performed at the University of Salamanca, and all procedures and experimental protocols were in accordance with the guidelines of the European Communities Directive (86/609/EEC, 2003/65/EC and 2010/63/EU) and the RD 53/2013 Spanish legislation for the use and care of animals. All the details of the study were approved by the Bioethics Committee of the University of Salamanca (ref# USAL-ID-195).

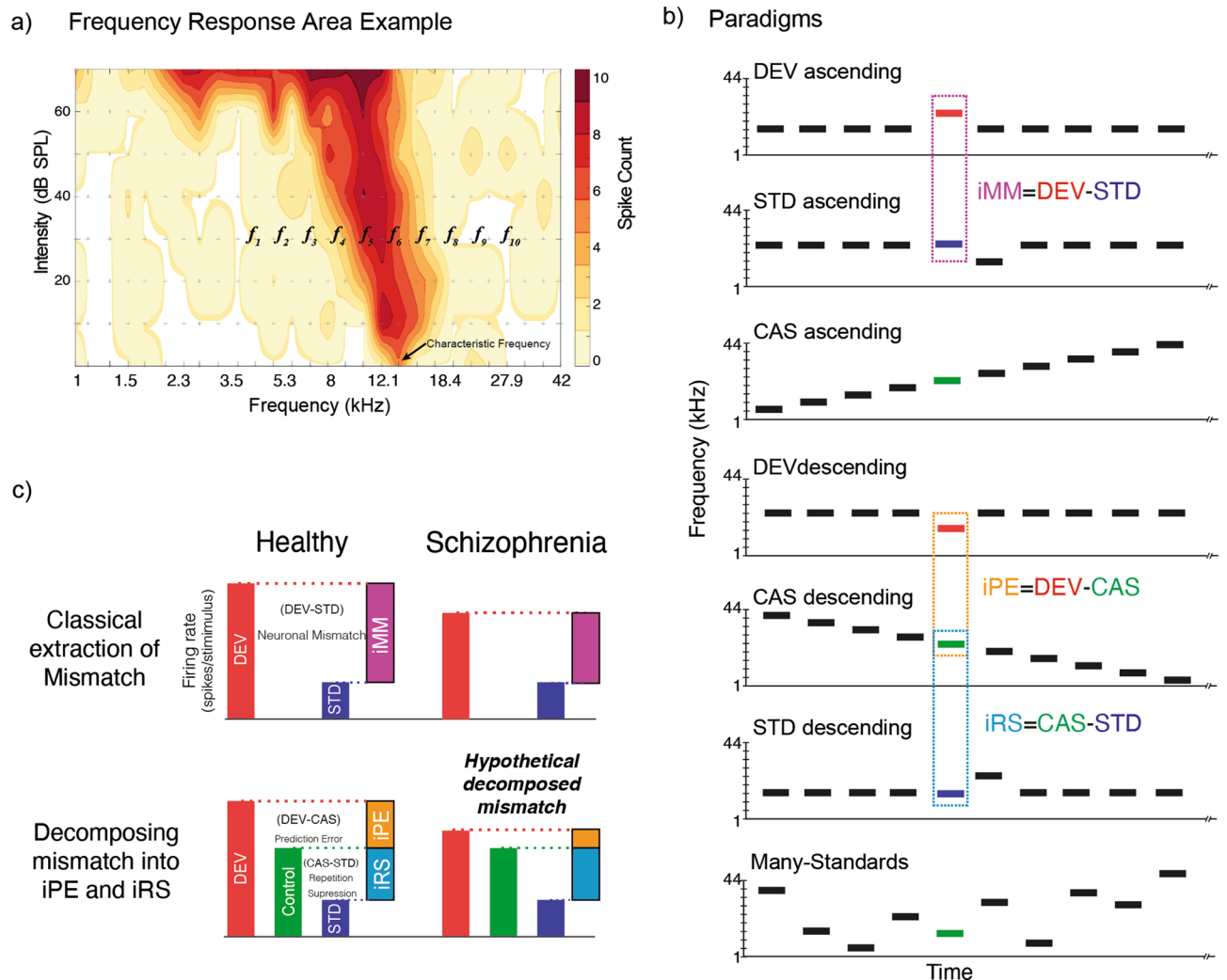


Figure 1. Experimental design. **(a)** Frequency response area example, with a representation of the ten selected tones to build the experimental paradigms. **(b)** Stimulation sequences, the same tone could be presented in different experimental paradigms, thus we can compare same tone in different contexts to control adaptation and deviance detection; and conform the indices of neuronal mismatch (iMM), prediction error (iPE) and repetition suppression (IRS). Note that ascending and descending tones will be compared to the control ascending or descending, respectively. **(c)** Sketch of summary results of mismatch responses for healthy and schizophrenia subjects under the classical analysis of mismatch. Second row decomposition of neuronal mismatch, under the assumption of predictive coding framework in healthy subjects, and the hypothetical decomposition of neuronal mismatch into prediction error and repetition suppression in schizophrenia.

Surgical procedures. Anesthesia was induced and maintained with urethane (1.5 g/kg, i.p.), with supplementary doses (0.5 g/kg, i.p.) given as needed. Dexamethasone (0.25 mg/kg) and atropine (0.1 mg/kg) were administered at the beginning of the surgery to reduce brain edema and bronchial secretions, respectively. Isotonic glucosaline solution was administered periodically (5–10 ml every 6–8 h, s.c.) to avoid dehydration. During all experimental procedures, animals were artificially ventilated, and CO₂ and temperature monitored^{37–39}.

The initial procedure was the same in each case, and the subsequent procedures differed only in the craniotomy location, and the placement/orientation for the recording electrode (animals per group/location: control MGB = 16, AC = 9; MK-801 MGB = 15, AC = 8). For MGB recordings, a craniotomy (~2 × 2 mm, from –5 to –6.5 mm Bregma and –3.5 mm lateral) was performed in the left parietal bone, the dura was removed, and the electrode advanced in a vertical direction⁴⁰. For AC recordings, the skin and muscle over the left temporal bone was retracted and a 6 × 5 mm craniotomy was performed (between –2 and –6 from Bregma) over the temporal bone⁴¹ dura was removed and the area was covered with a thin, transparent layer of agar to prevent desiccation and stabilize recordings. Electrodes for AC recording were inserted using a triple-axis micromanipulator (Sensapex), forming a 30° angle with the horizontal plane, to penetrate through all cortical layers of the same cortical column.

For this study, animals in MK-801-treated group receive a systemic intraperitoneal injection (0.1 mg/kg) of a noncompetitive NMDA-R antagonist (MK-801 hydrogen maleate, M107 Sigma-Aldrich). Control animals did not receive any injection.

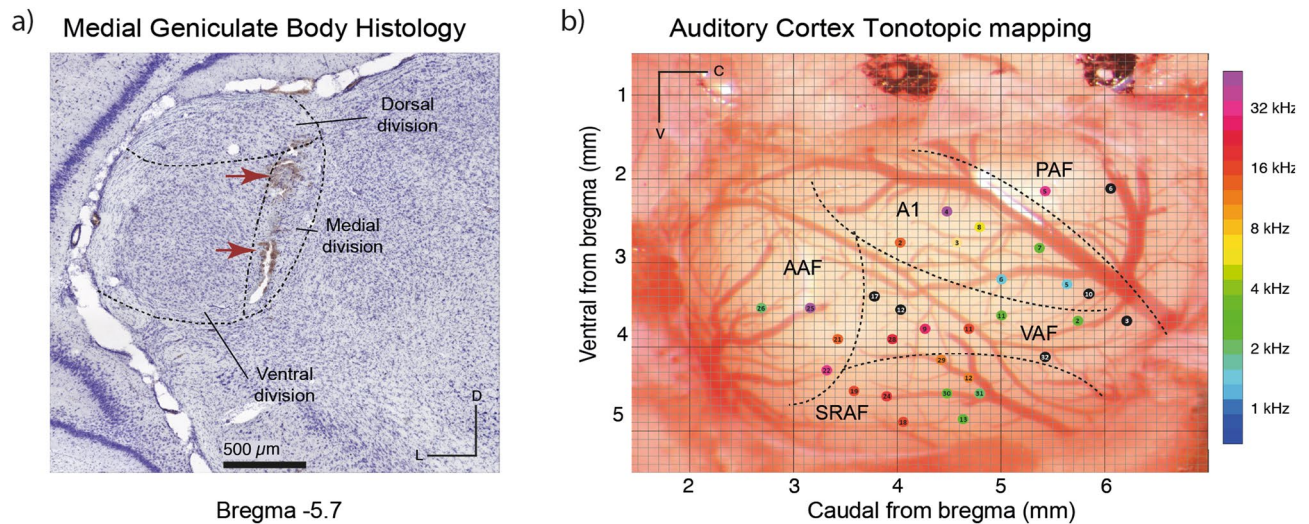


Figure 2. Anatomical recordings location. (a) Photomicrograph sample of a MGB Nissl stained slice (10x), red arrows point the two electrolytic lesions. (b) Example of localization all recordings made in the AC of one rat, each colored dot represents the characteristic frequency of each performed tract. A1: Primary Auditory Field; AAF: Anterior Auditory Field; VAF: Ventral Auditory Field; PAF: Posterior Auditory Field and SRAF: Suprarhinal Auditory Field.

Electrophysiological recording procedures. During all procedures, animals were placed in a stereotaxic frame fixed with hollow specula ear bars that housed the sound delivery system. One single neuron and local field potential (LFP) was recorded at a time, using the same tungsten electrode (1–4 M Ω) inserted into a single auditory station (MGB or AC) in each individual animal. The signal recorded was pre-amplified (1000 \times) and band-pass filtered (1–3000 Hz) with a medusa preamplifier (TDT). This analog signal was digitalized 12 k sampling rate and further band-pass filtered (TDT-RX6) separately for spikes (500 Hz–3 kHz) and LFP (3–50 Hz). We used short trains of white noise bursts (30 ms, 5 ms rise-fall ramps) to search for neuronal activity. To prevent neuronal adaptation during the search, some parameters (frequency and intensity) and stimulus type (white noise, pure tone) were manually varied. Once a single neuron was isolated a frequency–response area (FRA) of the response magnitude for each frequency/intensity combination was first computed (Fig. 1a). A randomized sequence of pure tones (from 1 to 44 kHz) was presented at a rate of 4 Hz, with varying frequency and intensity, and with 3 repetitions of all tones.

For each animal treated with MK-801 the first single neuron was recorded ~15 min after the drug injection⁴². Ten evenly-spaced pure tones (0.5 octaves separation) at a fixed sound intensity (usually 20–30 dB above the threshold) were selected to each neuron recorded to create the control sequences, cascade and many-standard^{11,36}, and additionally, adjacent pairs of them were used to present various oddball sequences (Fig. 1b). All sequences were 400 tones in length (75 ms duration, 5 ms rise-fall ramp and 250 ms interstimulus interval), each tone in the control sequences was played 40 times, with the same overall presentation rate as deviants in the oddball sequence.

Oddball sequences were used to test the specific contribution of deviant tones in an adaptation context. An oddball sequence consisted of a repetitive tone (standard 90% probability), occasionally replaced by a tone of a different frequency (deviant 10% probability), in a pseudorandom manner. We used two types of control sequences: the many-standard and cascade sequences. Both contained the same 10 frequencies but differing in the order of presentation. In the many-standard control, the 10 frequencies were randomly presented, mimicking the presentation rate and the unpredictability of the deviant tones, while cascades were played always in the same presentation order, ascending or descending in frequency. Hence the cascade contains a regularity and mimics the presentation rate of deviant sounds but in a predictable context and consequently does not violate a regularity whereas the many-standard control mimics the presentation rate of the deviant sounds but contained no regularity that could be modelled nor violated. These four conditions, and by extension responses to them, will be denoted as deviant (DEV), standard (STD), cascade (CAS) and many-standard (MSC) (Fig. 1b). Finally, if the neuron could be held for long enough, the same protocol was repeated for different frequencies and/or intensity.

Anatomical location. For MGB recording localization, at the end of each tract and experiment, two electrolytic lesions were made to mark the end and the beginning of the auditory signal (Fig. 2a). Then, animals were given a lethal dose of sodium pentobarbital and perfused transcardially with phosphate-buffered saline (0.5% NaNO₃ in Phosphate Buffered Saline) followed by a fixative mix of 1% paraformaldehyde and 1% glutaraldehyde. After fixation and dissection, the brain was cryoprotected in 30% sucrose and sectioned into 40 μ m slices. Sections were Nissl stained with 0.1% cresyl violet. Recording sites were marked on images from an adult rat brain atlas⁴³ and neurons that were recorded from were assigned to one of the main divisions of the MGB (dorsal,

medial or ventral). This information was complemented and confirmed by the stereotaxic coordinates as well as the depth of the neuron within a tract.

For the AC experiments, a magnified picture (25×) of the exposed cortex and the Bregma references was taken at the end of the surgery with a digital single-lens reflex camera (D5100, Nikon) coupled to the surgical microscope (ZEISS). The picture was overlapped to guide and mark each electrode placement into a micrometric grid (250–500 μm spacing; Fig. 2b). Then we performed several tracts recording multi-unit activity frequency response area (FRA), the characteristic frequency arising from each FRA was placed over the picture, resulting in a characteristic frequency map of each animal. Boundaries were identified following the changes in the tonotopic gradient: high-frequency reversal between the ventral and anterior auditory fields (rostrally), low-frequency reversal between primary and posterior auditory field (dorsocaudally) and high-frequency reversal between ventral and suprarhinal auditory field (ventrally)⁴¹. Then, each recording was located in one of these five fields.

Statistical analysis. All the data analyses were performed with MATLAB software, using the built-in functions, the Statistics and Machine Learning toolbox, or custom scripts and functions developed in our laboratory. To test for significant excitatory responses to tones we used a Monte Carlo approach, simulating 1,000 peristimulus time histogram (PSTH) using a Poisson model with a constant firing rate equal to the spontaneous firing rate (SFR). A null distribution of baseline-corrected spike counts was generated from this collection of PSTH. Lastly, the *p*-value of the baseline-corrected spike count was empirically computed as $p = (g + 1)/(N + 1)$, where *g* is the count of null measures greater than or equal to baseline-corrected spike count, and *N* = 1,000 is the size of the null sample. Finally, we only included in the analysis neuron/frequency combinations with significant excitatory response ($p > 0.05$) after the baseline-corrected spike count to at least one of the conditions (DEV, STD, CAS). PSTH was used to estimate the spike-density function (SDF) over the time, showing action potential density over time (in action potentials per second) from –75 to 250 ms around stimulus onset, for the 40 trials available for each tone and condition (DEV, STD, CAS), smoothed with a 6 ms gaussian kernel (“ksdensity” function in Matlab) in 1 ms steps. The baseline SFR was determined as the average firing rate during the 75 ms preceding stimulus onset.

The excitatory response was measured as the area below the SDF and above the baseline SFR, between 0 and 180 ms after stimulus onset (positive area patches only, to avoid negative response values). This measure will be referred to as “baseline-corrected spike count”.

Baseline-corrected spike count responses of a neuron to the same tone in the three conditions (DEV, STD, CAS) were normalized using the formulas:

$$DEV_{\text{Normalized}} = DEV/N;$$

$$STD_{\text{Normalized}} = STD/N;$$

$$CAS_{\text{Normalized}} = CAS/N;$$

where $N = \sqrt{DEV^2 + STD^2 + CAS^2}$, is the Euclidean norm of the vector (DEV, STD, CAS) defined by the three responses. Similar indices were calculated using the many-standard control sequence, but the outcomes were identical with one exception as described in results and therefore the reported analyses focused on CAS. Normalized values were the coordinates of a 3D unit vector ($DEV_{\text{Normalized}}$, $STD_{\text{Normalized}}$, $CAS_{\text{Normalized}}$) with the same direction of the original vector (DEV, STD, CAS), and thus the same proportions between the three response measures. This normalization procedure always results in a value ranging from 0 to 1, and has a straightforward geometrical interpretation.

From these normalized responses, indices of neuronal mismatch (iMM), repetition suppression (iRS), and prediction error (iPE) were computed as:

$$iMM = DEV_{\text{Normalized}} - STD_{\text{Normalized}};$$

$$iPE = DEV_{\text{Normalized}} - CAS_{\text{Normalized}};$$

$$iRS = CAS_{\text{Normalized}} - STD_{\text{Normalized}};$$

These indices, consequently, always range between –1 and 1, and provide the following quantitative decomposition of neuronal mismatch into repetition suppression and prediction error: $iMM = iRS + iPE$. To test these indices over time, we divided the whole response into 12-time windows, 20 ms width, from –50 to 190 ms with respect to the stimulus onset. Then, we compared each time window against zero using a sign-rank test, false discovery rate (FDR = 0.1) corrected for the 12 windows.

For the analysis of the LFP signal, we aligned the recorded wave to the onset of the stimulus for every trial, and computed the average LFP for every recording site and stimulus condition (DEV-LFP, STD-LFP and CAS-LFP), as well as the differences between them, resulting in the three LFP-indices: “neuronal mismatch” (MM-LFP = DEV-LFP – STD-LFP), “prediction error” (PE-LFP = DEV-LFP – CAS-LFP) and “repetition suppression” (RS-LFP = CAS-LFP – STD-LFP). Then, grand-averages were computed for all conditions and auditory station separately. The *p*-value of the grand-averaged for the three LFP-indices (MM-LFP, PE-LFP and RS-LFP) was determined for every time point with a two-tailed *t*-test (FDR corrected).

Our data set was not normally distributed, so we used distribution-free (non-parametric) tests. These included the Wilcoxon signed-rank test and Friedman test (for baseline-corrected spike counts, normalized responses, indices of neuronal mismatch, repetition suppression and prediction error). Only the difference wave for the

	Control				MK-801			
	MGB		AC		MGB		AC	
	L	NL	L	NL	L	NL	L	NL
# Neurons	28	38	40	37	44	42	37	24
# Points/required	111/72	240/224	295/87	309/29	156/81	228/544	163/21	94/7
DEV (spk)	0.7249	0.6805	0.9594	0.9694	0.5970	0.6723	1.0978	1.6450
STD (spk)	0.1500	0.1504	0.2363	0.2103	0.0338	0.0837	0.0906	0.1114
CAS (spk)	0.8292	0.5601	0.7719	0.5910	0.7329	0.7889	0.5913	0.5978
	Cascade vs. many-standard controls analysis (median and Wilcoxon signed-rank values)							
Many-standard	0.8982	0.6499	0.8034	0.5237	0.7855	0.9966	0.5109	0.6861
Cascade	0.7625	0.5601	0.7720	0.5911	0.7326	0.7889	0.5913	0.5979
<i>P</i> value	<i>0.2231</i>	<i>0.1567</i>	<i>0.8266</i>	<i>0.3288</i>	<i>0.4103</i>	<i>0.0286</i>	<i>0.2543</i>	<i>0.0830</i>
	Friedman test analysis							
iMM	0.4240	0.5169	0.5283	0.6073	0.6075	0.5578	0.7734	0.8699
<i>P</i> value	1.01⁻⁰⁹	2.96⁻²⁹	7.52⁻⁵¹	7.90⁻⁵⁶	6.96⁻²⁴	5.98⁻³⁸	1.63⁻⁴¹	2.34⁻³⁰
iPE	-0.0950	0.0492	0.1221	0.2734	-0.0633	-0.0445	0.3723	0.5788
<i>P</i> value	0.0130	0.0199	0.0012	3.29⁻¹²	0.0092	<i>0.5120</i>	1.88⁻⁰⁷	8.84⁻¹³
iRS	0.5192	0.4678	0.4062	0.3339	0.6707	0.6023	0.4011	0.2910
<i>P</i> value	8.63⁻¹⁸	5.55⁻¹⁹	5.99⁻³²	1.68⁻¹⁸	7.48⁻³⁷	9.89⁻⁴²	1.16⁻¹⁶	1.68⁻⁰⁵
	Indices using many-standard							
iPE (DEV-MSC)	-0.0981	0.0374	0.0652	0.2296	-0.0971	0.0618	0.3609	0.5788
<i>P</i> value	0.0039	<i>0.1978</i>	0.0464	9.70⁻¹⁰	<i>0.0894</i>	<i>0.3198</i>	2.81⁻⁴⁷	8.84⁻¹³
iRS (STD-MSC)	0.4291	0.4401	0.4335	0.3679	0.6113	0.5930	0.3833	0.2910
<i>P</i> value	1.61⁻¹⁴	2.19⁻³³	1.67⁻⁴³	6.06⁻²⁸	9.69⁻¹⁰	1.2820⁻⁰⁸	5.08⁻¹⁶	1.68⁻⁰⁸

Table 1. Spike population analysis¹. ¹Spike population analysis for each experimental group and auditory station independently: First row, number of recorded neurons; second row number of tested neuron/frequency combinations (points), along with estimated minimum sample size (of points) required for statistical power (see “Material and methods”). Followed by median values for base-line corrected spike count (spikes) to the different conditions. Comparative analysis for control paradigms, median values, and Wilcoxon signed-rank test values for each station and group. Median indices of neuronal mismatch (iMM), prediction error (iPE) and repetition suppression (iRS), and their corresponding *p* value. Significant values are in “bold”. *p* values are in “italic”.

LFPs were tested using a *t*-test, since each LFP trace is itself an average of 40 waves. For multiple comparison tests, *p* values were FDR corrected using the Benjamini–Hochberg method. Linear models were used to test for significant average iMM, iPE and iRS within each auditory station. Significant effects of station, pathway, and interactions between them were fitted using the ‘fitlm’ function in Matlab, with robust options. To estimate final sample sizes required for the observed effects after the initial exploratory experiments, we used the ‘sampsizempwr’ function in Matlab adjusted for the iPE for each region, to obtain a statistical power of 0.8 for this index. Sample sizes were enlarged with additional experiments until they were just greater than the minimum required (number of points recorded, and the minimum required for each station; see Table 1).

To analyze the time course of adaptation, we computed an averaged time course for all the standard stimuli presented^{41,44}. Then, we fitted a power-law function with a three-parameters model, $y(t) = a \cdot t^b + c$, where *a* indicates the response’s beginning or the first spike strength; *b* the sensitivity to repetitive stimuli, or the adaptation velocity, and *c* the steady-state response. *R*² values indicated that the model fits very well for standard responses in both groups, explaining between 60 and 78% of the response variability within all regions.

To analyze spikes differences between MK-801 and control group, we computed the median values for each condition tested (DEV, STD and CAS) and their differences (iMM, iRS and iPE) and calculated a ranksum test. To compare each time window between groups a two-sample *t*-test (from 0 to 200 ms, Bonferroni corrected for 200 comparisons with family-wise error rate FWER < 0.05) was used for the SDF and LFPs to each stimulus condition and indices, using the ‘ttest2’ function in Matlab, for every time point.

Results

We recorded a total of 290 well-isolated neurons, 143 from the control group (25 animals) and 147 from the MK-801-treated group (23 animals). One single neuron and local field potential (LFP) was simultaneously recorded at a time, using the same tungsten electrode. Recordings were performed in the medial geniculate body (MGB) and in the auditory cortex (AC) while playing oddball and control sequences (many-standards and cascade: CAS) in anesthetized rats. Thus, the same tone was played as DEV, STD, CAS and many-standards and using an ascending or descending sequence for the cascade control. This methodological configuration allowed us to calculate indices that conform to the classical mismatch index controlling for tone characteristics in different contexts

	MGB		AC	
	L	NL	L	NL
STD_control	0.1912	0.1717	0.1990	0.1856
STD_MK-801	0.0537	0.1047	0.0689	0.0547
<i>P</i> value	<0.000	<0.000	<0.000	<0.000
DEV_control	0.6153	0.6887	0.7274	0.7930
DEV_MK-801	0.6611	0.6620	0.8424	0.9247
<i>P</i> value	0.2309	0.2641	<0.000	<0.000
CAS_control	0.7104	0.6395	0.6052	0.5196
CAS_MK-801	0.7244	0.7063	0.4701	0.3458
<i>P</i> value	0.1169	<0.000	<0.000	<0.000
iMM_control	0.3675	0.4897	0.5124	0.5781
iMM_MK-801	0.5197	0.5221	0.7269	0.8088
<i>P</i> value	<0.000	0.0409	<0.000	<0.000
iPE_control	-0.0670	0.0513	0.1060	0.2697
iPE_MK-801	-0.0502	-0.0444	0.3592	0.5652
<i>P</i> value	0.9622	0.0035	0.000	<0.000
iRS_control	0.5300	0.3672	0.3350	0.2935
iRSdrug	0.6812	0.5632	0.3514	0.2765
<i>P</i> value	<0.000	<0.000	0.5800	0.8934

Table 2. Firing rate comparisons¹. ¹Comparative analysis between control and MK-801 group. Median spikes to the former measures responses to standard (STD), deviant (DEV) and cascade (CAS) tones, and their corresponding *p* value (ranksum test). Similarly, medians and their associates *p* value for the index of mismatch (iMM), index of prediction error (iPE), and index of repetition suppression (iRS). Significant *p* values are in “bold”

	MGB		AC	
	L	NL	L	NL
STD_control	0.0270	0.4795	1.6962	2.6827
STD_MK-801	0.0242	0.4969	1.0017	1.7739
<i>P</i> value	0.159	0.383	0.050	0.006
DEV_control	0.3301	0.3304	1.5840	2.4364
DEV_MK-801	0.3117	0.3769	0.9868	1.2602
<i>P</i> value	0.994	0.626	0.009	<0.000
CAS_control	0.3342	0.2962	1.2965	1.6388
CAS_MK-801	0.3442	0.2772	0.9452	1.5063
<i>P</i> value	0.890	0.580	0.084	0.987

Table 3. Spontaneous firing rate comparisons¹. ¹Comparative SFR analysis. Median values for averaged SFR to standard (STD), deviant (DEV) and cascade (CAS) tones, and their corresponding *p*-value (ranksum test). Significant *p* values are in “bold”.

(Fig. 1b). To confirm the exact recording location, we mapped the AC surface and perform electrolytic lesions in MGB (Fig. 2). Since we found no statistically significant differences when we compare mean baseline-corrected spike counts between the use of the cascade and many-standards sequences for the control group and MK-801 group, except for the MGB_{NL} from the MK-801 group (Table 1: Cascade vs. many-standard controls analysis, $p > 0.05$ within all fields and groups, except for the MGB_{NL} from the MK-801 group where $p = 0.0286$), the CAS sequence was chosen to control for repetition effects. This is because the CAS paradigm not only controlled for the presentation rate of the deviant stimuli but also the frequency difference (ascending or descending, Fig. 1b) between standards and deviants in the oddball sequences⁴⁵.

Effects of MK-801 on the neuronal firing rate. MK-801 injection significantly reduced the responses to STD tones within all regions. By contrast, for responses to the DEV tones, we observed a significant increment in responses in AC but not for the MGB. Table 2 shows a comparative analysis of the firing rate to each stimulus condition for each group. When the firing rate of the cascade sequence was considered, MK-801 differentially affected the AC and MGB such that CAS responses were significantly increased in the MGB_{NL} but decreased in AC (Table 2). This suggests that MK-801 may have different effects in the thalamus and cortex depending on the context of the stimulus. Furthermore, in order to test whether MK-801 affected spontaneous activity, we com-

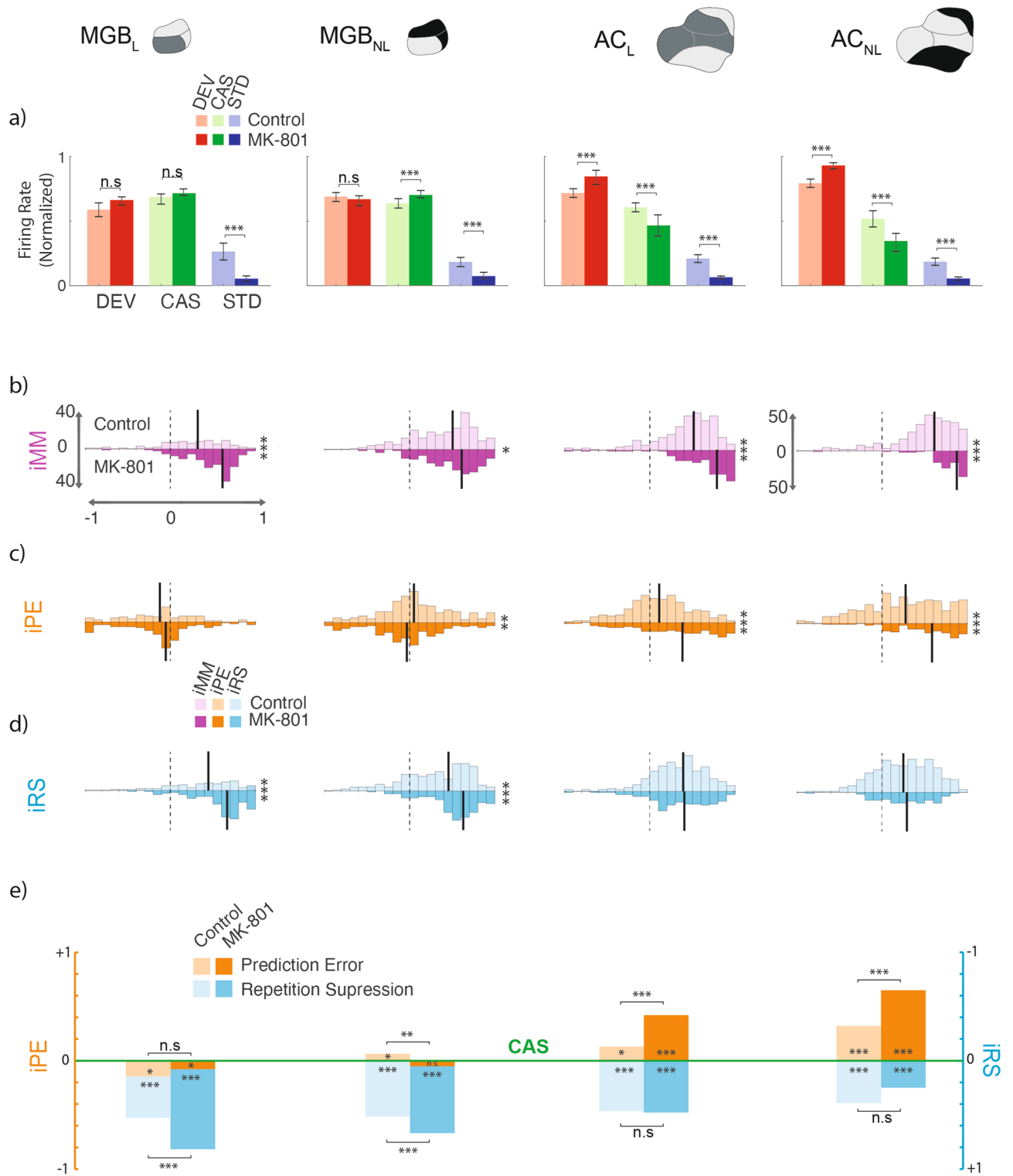


Figure 3. Single neuron spikes population analysis. Results for firing rate analysis and their computed differences along the thalamocortical axis. **(a)** Boxplot of median normalized responses for deviants (red), cascade (green) and standard (blue) for each group, control (light colors) and MK801 (bright colors), within each station and the statistical significance between groups (Wilcoxon signed-rank test, * $p < 0.05$, ** $p < 0.001$, *** $p < 0.000$). **(b–d)** Indices histograms displayed in a mirror-like manner for the two groups (controls upper and in light colors; MK801 under and in bright colors), showing the distribution of the three indexes for each neuronal response (ranging between -1 and +1, dotted lines indicate index = 0). Vertical solid lines indicate their medians and the significant difference between groups is noted at the right of each histogram block. **(e)** Median indices of Prediction Error (orange) and Repetition Suppression (blue), represented with respect to the baseline set by the cascade control (green line). Thereby, iPE upwards-positive while iRS is downwards-positive. Each median index corresponds to differences between normalized responses in **(a)**. Asterisks inside bars denote statistical significance of these indices against zero (Friedman test), while asterisks outside bars denote statistical significance between groups (Wilcoxon signed-rank test, * $p < 0.05$, ** $p < 0.001$, *** $p < 0.000$).

puted a comparative analysis for SFR. MK-801 decreased the SFR for DEV and STD tones in the AC, but not in the MGB (Table 3). Figure 3a, illustrates a boxplot showing the median normalized responses to each stimulus condition and group. The statistical significance of between group comparisons reveals that MK-801 reduced the firing rate to repetitive stimuli within all fields, while increased the responses to unexpected sounds in the AC. These results reveal a differential effect of MK-801 on the refractoriness and salience of infrequent events at the single neuron level.

Effects of MK-801 on neuronal mismatch and its components. Next, we analyzed the differences between these normalized responses and computed three indexes: (1) the iMM, similar to the typical SSA index used in previous single neurons studies; (2) the iPE, that shows the relative enhancement of DEV tones compared with CAS tones and (3) iRS that reflects the level of response suppression due to the repetition effect.

The analysis of the iMM after the injection of MK-801 demonstrated that iMM values are significantly different from zero for all recording sites (Fig. 3b, Table 1: Friedman test). But when comparisons between groups were considered, the analysis revealed that MK-801 increased the neuronal iMM (Fig. 3b-iMM; Table 2). As described above, these changes are mainly due to a reduced response to STD tones in all recording locations and an enhanced response to DEV in the AC.

Since $iMM = iRS + iPE$, an essential advantage of these metrics is that we can determine how much of the mismatch index is due to the regularity of the context (RS) and/or to the occurrence of an infrequent event (PE). Thus, to determine which of these two components of the iMM is affected by MK-801, we computed the indices of iPE and iRS separately.

Interestingly, MGB neurons in the MK-801 group did not show any sign of genuine deviance detection, as iPE values were negative and close to zero. While both AC showed a significant positive iPE (Fig. 3c; iPE values in Table 1). When the comparison between groups was analyzed, an increased iPE for the MK-801 group in the AC was found, and even a further decreased iPE for the MGB_{NL} in the MK-801 group (Fig. 3c,e light and bright oranges; iPE in Table 2). These data suggest that the MK-801 produces an augmentation of saliency for novel stimuli processed in the AC.

Yet, the detection of rare or novel stimuli requires the establishment of a regular context or pattern. Therefore, we were also interested in finding out if the refractoriness due to regularity was altered by MK-801. We calculated the iRS by assessing the response of the same tone when it was presented as CAS, with a 10% probability in a regular pattern and presented as STD with a probability of 90%, within an oddball paradigm, so it is in a much more regular context^{8,36}. In both cases, we assume some level of regularity adaptation, but only a genuine repetition suppression can be determined if the responses to STD tones are lower than responses to CAS. Our results demonstrate that there is a significant repetition suppression effect in the MK-801 group along the thalamocortical pathway (Fig. 3d bright blue; iRS in Table 1). The analysis also revealed that MK-801 produced a significant increase in repetition suppression at thalamic level but did not affect repetition suppression in the AC when compared with controls (Fig. 3d,e light and bright blues; results in Table 2).

At this juncture, it is interesting to mention that although we used as a general rule the CAS, the response to MSC and CAS within the MGB_{NL} are statistically different (median values to CAS = 0.7889 and MSC = 0.9966, $p < 0.05$ Wilcoxon signed-rank; Table 1, cascade vs. many-standard controls analysis), showing more reduced or adapted response to CAS than the MSC. Nevertheless, we also performed the analysis of the indices using the MSC as the control paradigm. Results using MSC to calculate the indices (iPE = DEV-MSD and iRS = MSC-STD) show statistical differences for iRS within all conditions, while when the MSC was used to calculate the iPE results do not show statistical differences within the MGB_{NL} in both groups (see Table 1, indices using many-standard control). These outcomes suggest that MGB_{NL} is a much complex region that we originally anticipated, and MK-801 is especially affecting their responses for the iPE as we can see in Fig. 3e “MGB_{NL}” where we noticed that MK-801 produced a significant reduction of the iPE. Similar results using MSC in anesthetized rats were already observed in our previous study¹¹; so it seems a robust and reliable result. A plausible explanation is that MK-801 differentially affects the neuronal responses in the dorsal and the medial divisions of the MGB, i.e., the two areas that include MGB_{NL}. Indeed, previous studies has suggested that these two regions show anatomically and physiologically different properties^{46–48}.

These results, in general show that the auditory thalamus and cortex differ in the way repetition effects and prediction errors are processed. To confirm this hypothesis and considering that we have previously found an increase in the level of iPE along the thalamocortical hierarchy in awake and anesthetized animals¹¹, we fitted a linear model to determine the effect of MK-801 on the degree of increase in iPE along the auditory hierarchy relative to the control (urethane) condition. Using station (S: MGB vs. AC), drug (D: Control vs. MK-801) and pathway (P: Lemniscal vs. Non-lemniscal) and their interactions as factors, with control MGB_L as reference level for these factors, the fitted model is as follows:

$$iPE = -0.099 - 0.052D + 0.16P + 0.216S - 0.032DP \\ + 0.297DS + 0.003SP + 0.1490DPS.$$

Next, we applied an ANOVA to this model and found a significant effect of station ($F = 209.24$, $p = 1.21 \times 10^{-44}$), drug ($F = 10.82$, $p = 0.001$), pathway ($F = 42.93$, $p = 7.66 \times 10^{-11}$) and for the interaction drug \times station ($F = 37.9$, $p = 9.41 \times 10^{-10}$) but not for the interactions of drug \times pathway ($F = 0.45$, $p = 0.5011$) nor station \times pathway ($F = 0.004$, $p = 0.9488$), nor the three-way interaction ($F = 2.37$, $p = 0.1236$). That is, there is a significant station effect (iPE is larger overall at AC than MGB), pathway (iPE is larger overall in the non-lemniscal than the lemniscal pathway), and drug (iPE is increased overall with MK-801 vs. control) and a drug \times station interaction indicating that while iPE at AC is increased overall relative to MGB, the degree of iPE increase is moderated by MK-801. Inspection of Fig. 3e indicates that the significant station difference is in the direction of being larger

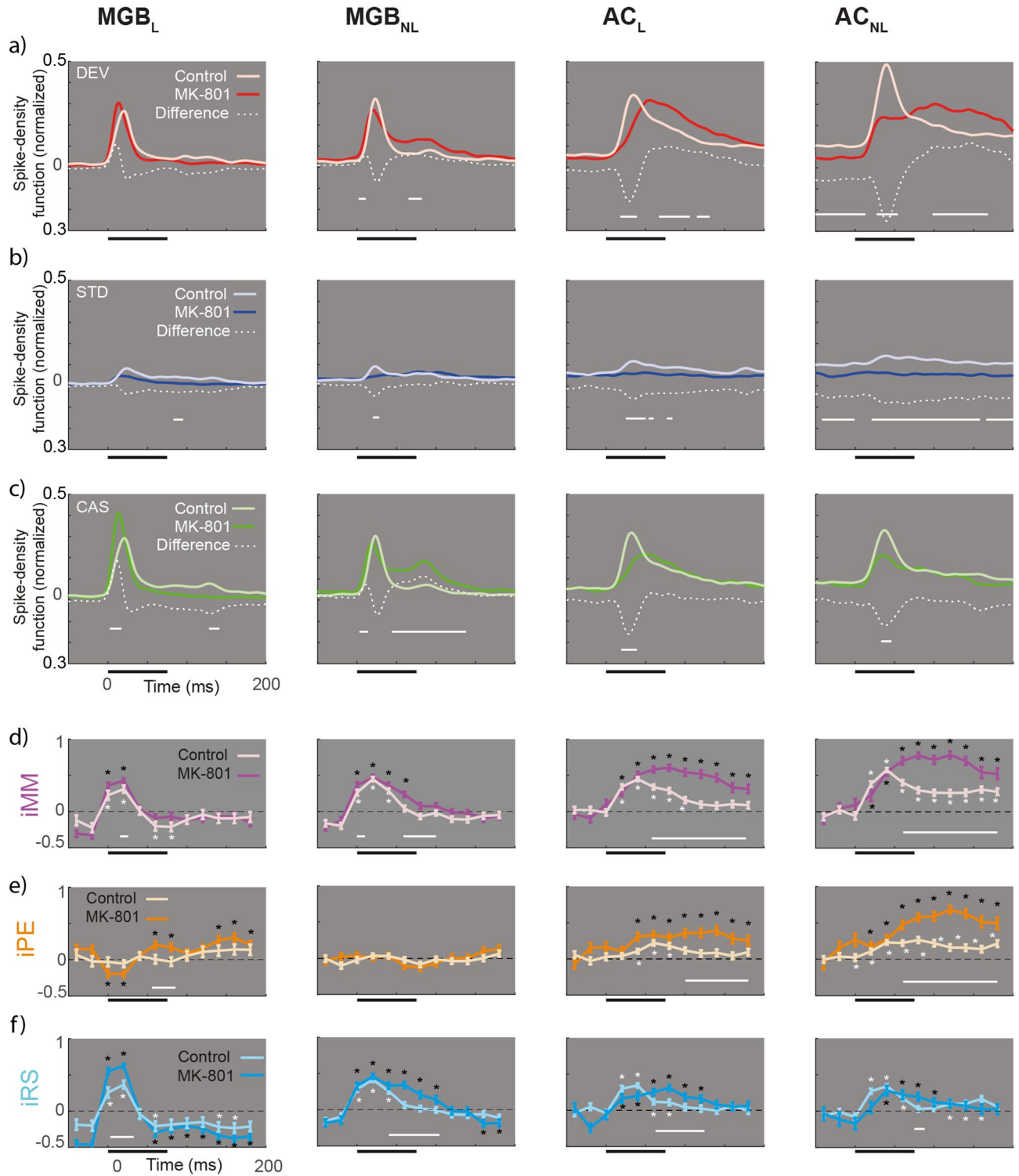


Figure 4. Spike Density Function. (a-c) Averaged firing rate profiles for each condition as normalized spike-density function (light colors for control and bright color for MK801 group), and their respective differences (white dotted lines). Solid horizontal white lines represent the time in which the difference between groups is significant (two-sample t test $p < 0.05$, Bonferroni corrected). (d-f) Indices over time computed for 12 intervals (from -50 to 190ms) compared against zero (signed-rank test and FDR corrected for 12 comparisons; $*p < 0.01$) for each group (light colors for control and bright color for MK801 group). Solid white lines denote differences between groups across time intervals (two-sample t test for each of the 12-time windows, $p < 0.05$).

under MK-801 than urethane. These results indicate that, indeed, the sensitivity to detect novel stimuli increases significantly more along the thalamocortical axis in the MK-801 than the control group (Fig. 3e, iPE in orange). We also fitted a similar linear model to iRS. The resulting model was:

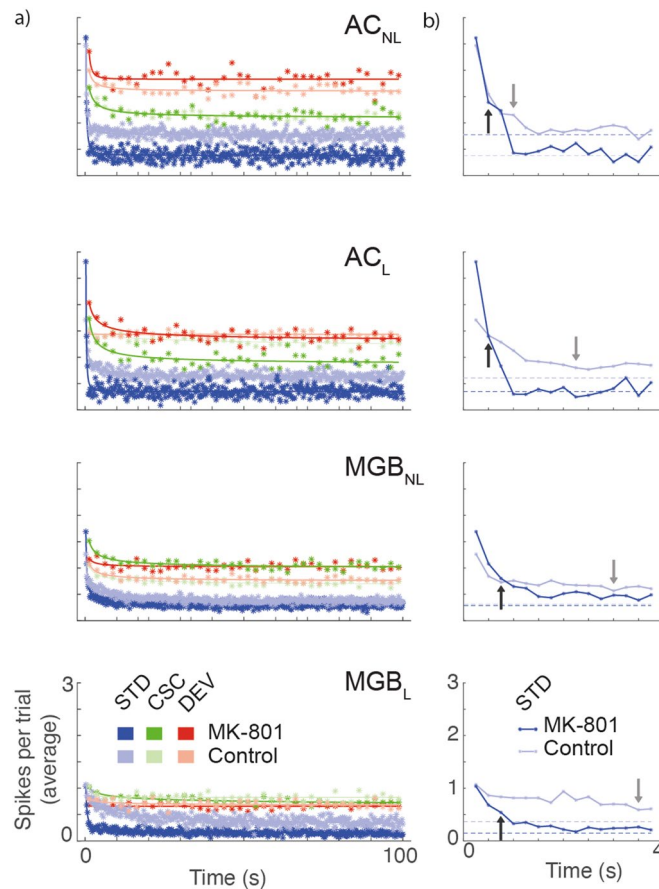


Figure 5. Time course for dynamical thalamocortical adaptation. (a) Averaged time course for the stimulus played in relation to the time elapsed from the beginning of the sequence. (b) The first fifteen standard stimuli showing the three parameters of the power law fitted: a = initial average response; b = adaptation velocity; and c = the steady-state value (dotted lines) for each group. Arrows represent the 50% of the initial responses demonstrating faster adaptation in the MK801 group and the break down in the dynamical hierarchy of adaptation.

$$\begin{aligned} \text{iRS} = & 0.467 + 0.167D - 0.118P - 0.125S + 0.01DP \\ & - 0.159DS + 0.0405SP - 0.0424DPS. \end{aligned}$$

ANOVA demonstrated a significant effect for drug ($F = 26.42$, $p = 3.08 \times 10^{-7}$), station ($F = 80.52$, $p = 7.89 \times 10^{-19}$), pathway ($F = 24.65$, $p = 7.6 \times 10^{-7}$) and the interaction of drug \times station ($F = 17.61$, $p = 2.84 \times 10^{-5}$), but not for the interactions drug \times pathway ($F = 0.078$, $p = 0.7790$), station \times pathway ($F = 1.45$, $p = 0.2281$) and the three-way interaction ($F = 0.31$, $p = 0.5759$). Once again, these results indicate that while iRS was more marked at MGB than AC in general, this station difference was exacerbated with MK-801.

In summary, the changes described above demonstrate that NMDA-R antagonism has distinct effects on auditory scene analysis, as measured by the iPE and iRS, at different levels of the thalamocortical hierarchy.

Effect of MK-801 on spike-density function and indexes. Next, we sought to identify how MK-801 affected the temporal responses to auditory stimuli (DEV, STD and CAS) by comparing spike-density functions (SDF) to each condition between groups. The analysis revealed the latency of the main peak for the SDF to DEV tones was mostly unaffected by MK-801 in the MGB, but it was clearly delayed by 40 and 60 ms in the AC_L and AC_{NL}, respectively. Presumably, the spike count builds up more slowly following stimulus onset and then persists for longer. It is also very likely that MK-801 interact with other neuromodulatory systems including cholinergic, dopaminergic and serotonergic systems (see Discussion). Furthermore, the magnitude of the SDF was altered at the AC and MGB_{NL}, with the early component being reduced and the later sustained component being enhanced (Fig. 4a, horizontal white line for significant differences at $p < 0.05$). When the STD tones were considered, we observed a distinct and significant decrease of the SDF, mostly at the AC and only marginally at the subcortical levels (Fig. 4b). Finally, MK-801 affected mostly the initial responses to cascade tones in all regions, being reduced in the auditory cortex but earlier and increased in MGB_L (Fig. 4c). The sustained portion of the SDF was only significantly increased in the MGB_{NL}. Results show that MK-801 has a profound effect on the spike-density functions to DEV, STD and cascade stimuli.

Next, we studied where and when the MK-801 effect on the neuronal indices of iMM, iPE and iRS was significantly different from control. Thus, we examined whether in each group independently (MK-810 and control) these indices are different from zero, i.e., is there a significant iMM, iPE or iRS at each time point. Figure 4d–f highlights the significant time windows ($p < 0.01$) with white and black asterisks for control and MK-801, respectively. The analysis revealed that under MK-801, there was a significant iMM along the thalamocortical axis (between 20 and 40 ms for MGB_L, 20–80 ms in MGB_{NL} and from 20 to 190 ms in both AC; Fig. 4d, bright purple lines) and a significant iPE between 20 and 180 ms in both AC, and a late iPE in the lemniscal thalamus between 60–80 ms and 140–190 ms (Fig. 4e, bright orange lines). We also found significant thalamocortical iRS (Fig. 4f, bright cyan lines; between 20 and 40 ms for MGB_L, 0–100 ms in MGB_{NL}, from 20 to 120 ms in AC_L and between 40 and 100 ms in AC_{NL}).

When we compared the two groups, the analysis revealed that MK-801 produced a significant enhancement of iMM and iPE at both AC subdivisions ($p < 0.000$ for iMM between 60 and 190 ms in both AC; and $p < 0.05$ for iPE ranging between 100 and 190 ms in AC_L and between 60 and 190 ms in AC_{NL}; white horizontal lines in Fig. 4d–f). By contrast, iRS was affected more in the MGB ($p < 0.000$ between 5 and 35 ms in MGB_L; $p < 0.000$ between 40 and 110 ms in MGB_{NL}; $p < 0.05$ between 60 and 130 ms in AC_L; and $p < 0.05$ at 80 ms in AC_{NL}; white horizontal lines in Fig. 4f). Thus, MK-801 produces an increase of iMM and iPE mostly in the late time window in AC, while iRS is much affected in the MGB.

MK-801 affects the dynamics of adaptation. Since MK-801 lowered and flattened responses to STD tones across the response window, we sought to assess the dynamics and the time course of adaptation (Fig. 5a). Results show that the control group (light gray arrows) exhibit a hierarchical adaptation, becoming faster in higher-order areas (from top to down, responses reach the half of the initial values at the fourth, ninth, twelfth and fourteenth standard tone, respectively). By contrast, results from the MK-801 group exhibited much faster adaptation dynamics (Fig. 5b; 50% of the initial response occurred at the third and second standard tones in MGB and AC, respectively; b values for control group: MGB_L = -0.1769, MGB_{NL} = -0.4174, AC_L = -0.6824 and AC_{NL} = -1.175; and for MK-801 group: MGB_L = -0.8499, MGB_{NL} = -0.8853, AC_L = -1.712 and AC_{NL} = -1.418).

These data suggest that by blocking the NMDA-R, MK-801 exerted an inhibitory effect on responses, allowing adaptation to occur swiftly, and altering the timing across the hierarchical organization of the auditory system, resulting in the lemniscal thalamus having almost the same adaptation velocity as the non-lemniscal cortex (arrows in Fig. 5b). Furthermore, MK-801 reduces (almost by half) the steady-state plateau in the AC (dotted lines in Fig. 5b; c values for control group: MGB_L = 0.0776, MGB_{NL} = 0.2908, AC_L = 0.6084 and AC_{NL} = 0.7740; and for MK-801 group: MGB_L = 0.1428, MGB_{NL} = 0.2884, AC_L = 0.3523 and AC_{NL} = 0.3834).

All these results together support the idea that MK-801 produces a differential effect on adaptation and deviance detection along the thalamocortical axis, providing new evidence of a change in the firing pattern and temporal responses at single neuron level.

Delayed and broader larger-scaled LFP responses. Next, we wanted to check if the single unit responses correlated with larger-scale measurements of neuronal activity. The analysis of local field potentials (LFP) revealed that MK-801 produced significant changes in MGB_{NL} and AC (both in the lemniscal and non-lemniscal portions; Fig. 6). MK-801 shaped broader and longer responses for DEV-LFP and CAS-LFP in the auditory cortex. Although the waveforms of these LFPs were shifted in latency for the MGB_{NL} due to a progressive delay of N1, P1 and N2 (note that this terminology refers to the first negative peak, first positive peak and second negative peak). The N1, P1 and N2 delayed peaks occurs at 8, 14 and 57 ms for DEV-LFP and at 6, 26 and 45 ms for CAS-LFP (DEV-LFP: N1 peak for MK-801 = -6.6 μ V at 20 ms and control = -1.5 μ V at 12 ms; P1 peak for MK-801 = 6.9 μ V at 41 ms and control = 6.8 μ V at 28 ms; finally, N2 peak for MK-801 = -5.4 μ V at 102 ms and control = -10.2 μ V at 45 ms. CAS-LFP: N1 peak for MK-801 = -6.5 μ V at 18 ms and control = -1.2 μ V at 12 ms; P1 peak for MK-801 = 5.1 μ V at 53 ms and control = 10.6 μ V at 27 ms; finally, N2 peak for MK-801 = -5.0 μ V at 91 ms and control = -10.3 μ V at 45 ms).

Similarly, we also sought significant LFP signals for each computed index (Fig. 6d–f). The horizontal colored lines highlight the time at which significant deflections occur to each index-LFP for control and MK-801 groups independently (light and bright horizontal lines, respectively). Additionally, we compared these LFP indices between groups. The analysis of the MM-LFP shows that MK-801 elicited stronger and broader deflections within all regions (horizontal bright purple lines; Fig. 6) and abolished the late negative component (N2) in the AC (MGB_L: N2 = 114–157 ms; MGB_{NL}: N1 = 12–21 ms, P1 = 32–63 ms and N2 = 75–135 ms; AC_L: N1 = 10–57 ms and P1 = 60–147 ms; AC_{NL}: N1 = 20–53 and P1 = 60–144 ms). Our data also demonstrate that MK-801 produced a higher MM-LFP for virtually the whole LFP response within MGB_{NL} and both AC, while no differences occurred in MGB_L. This is consistent with our previous work where we demonstrated that neurons in the MGB_L show neither SSA⁴⁰ nor iMM¹¹. This is also in agreement with the roles of the lemniscal versus non-lemniscal pathways: the lemniscal is used for the transmission of straightforward sensory information, whereas the non-lemniscal pathway integrates this information.

Similar to the spike population analysis, and considering that the PE-LFP and RS-LFP both contribute to the MM-LFP, we also wanted to understand how MK-801 shapes the LFP for prediction error and repetition suppression. In response to MK-801, the PE-LFP waveform was reduced at the early component of the MGB_{NL}, while it was increased and delayed for the AC (orange horizontal lines in Fig. 6e). Moreover, MK-801 also abolished the N2 deflection (MGB_{NL}: N1 = 99–146 ms; AC_L: N1 = 30–65 ms and P1 = 87–180 ms; AC_{NL}: N1 = 30–67 and P1 = 106–180 ms). When PE-LFP was compared between groups, we only found differences in AC, mainly at the early (50–70 ms) and late components (120–180 ms). In other words, the lemniscal thalamus does not exhibit deviance detection, neither at the single neuron level nor at large-scale responses. Hence PE-LFP confirms

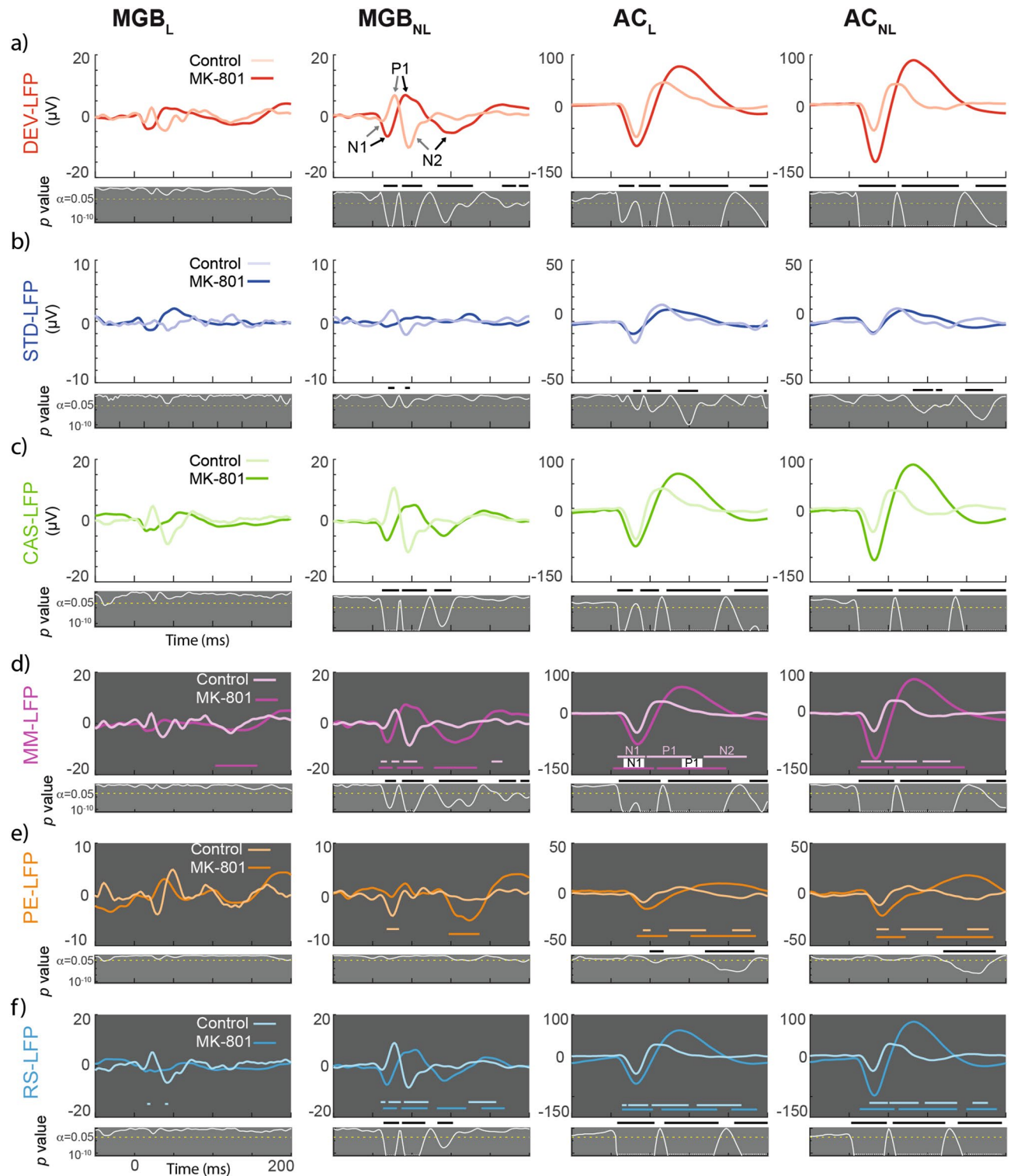


Figure 6. Local Field Potentials for each condition and their differences. (a-c) Population grand-averaged LFP for each condition recorded (CAS, DEV and STD) within each group (controls and MK801). Grey panels under the main LFP representations shows the instantaneous p value (white trace) of corresponding stimulus condition LFP (critical threshold set at 0.05 represented as a horizontal dotted yellow line). The thick black horizontal bars in figure 5a-c highlights the time interval for which the LFP comparison between the control and MK801 groups is significant. (d-f) Population grand-averaged LFP for and neuronal Mismatch (MM-LFP = $LFP_{DEV} - LFP_{STD}$), Prediction Error (PE-LFP = $LFP_{DEV} - LFP_{CAS}$), and Repetition Suppression (RS-LFP = $LFP_{STD} - LFP_{CAS}$) respectively. Colored horizontal lines denote significant deflections (t-test, FDR corrected). Grey panels show the instantaneous p value (white trace) of corresponding stimulus condition LFP (critical threshold set at 0.05 represented as a horizontal dotted yellow line) and black horizontal lines the time interval in which MK801 and control are statistically different.

single unit population data, where MK-801 produced greater levels of deviance detection in the auditory cortex (Fig. 3e).

Finally, MK-801 had similar effects on RS-LFP to those described above for MM-LFP and PE-LFP, eliciting broader and larger waveforms for MGB_{NL} and AC (Fig. 6f; MGB_{NL}: N1 = 10–28 ms, P1 = 34–63 ms and N2 = 73–108 ms; AC_L: N1 = 10–55 ms, P1 = 67–140 ms and N2 = 148–180 ms; AC_{NL}: N1 = 10–51, P1 = 55–132 ms and N2 = 141–180 ms). When differences between groups are considered, the non-lemniscal thalamus exhibited a shift in the waveform between 15 and 100 ms, while for the cortex, responses over virtually the whole temporal window were increased by MK-801.

Discussion

In this study, we demonstrate that the neuronal index of mismatch, derived from single-cell recordings, is profoundly affected along the auditory thalamocortical system in rats treated acutely with NMDA-R antagonist, MK-801. Importantly, we also reveal that the two elements that make up the index of mismatch, i.e., repetition suppression and prediction error, are differentially affected by MK-801 in single neurons at auditory thalamus and cortex. MK-801 increases repetition suppression in auditory thalamus and prediction error in auditory cortex. The increase in repetition suppression is more prominent in lemniscal areas of the auditory thalamus, while the increase in prediction error is more evident in the non-lemniscal areas of the auditory cortex. Furthermore, our results demonstrate that MK-801 alters the dynamics of neuronal adaptation along the thalamocortical axis, becoming faster and stronger especially at thalamic level. The results from single-unit data were confirmed by recordings of large-scale responses, LFPs, as the latter exhibit delayed and broader deflections. In summary, our work demonstrates that the MK-801 increase of the neuronal mismatch in the auditory cortex 60 ms after stimulus onset. This enhancement is due to the combined effect of an increment in the sustained responses to deviant tones and a decrement to standard tones. It should be noted that, in contrast to most previous studies using recording procedures to study neuronal population activity in rodents such as LFPs or EEG via skull screws, we have recorded single-unit activity, a technique that has a much higher resolution level at the single-cell level for revealing patterns of activity underpinning mismatch responses.

Differential effects of MK-801 on repetition suppression and prediction error in the thalamocortical pathway. It is well established that NMDA-R plays a fundamental role in neuronal plasticity, controlling long-term potentiation and depression⁴⁹. NMDA-R dependent plasticity is believed to underpin the capacity of the brain to adjust internal predictions and use the memory of recent past inputs to anticipate future stimuli⁵⁰. Further, it is generally accepted that human MMN is reduced after NMDA-R antagonist treatments because NMDA-R antagonist blocks synaptic plasticity, precluding the formation of a memory trace for the standard tones¹⁴. As we have seen in our results, MK-801 reduces responses to standard tones thus increasing repetition suppression.

Although this finding supports the hypothesis that NMDA-R antagonists alter sensory-memory formation⁵¹, the results that 0.1 mg/kg MK-801 treatment produces a significant increment in response to the deviant tones, in prediction error and hence, an increase in the neuronal mismatch, is in the opposite direction to expected. It is clear that the role of NMDA-R in the generation of MMN is considerably more complex than thought²². There have been suggestions in the literature of precedents for our observations⁵². Even considering that MK-801 has 160 times the affinity of ketamine to NMDA-R, necessitating higher ketamine doses for similar drug effect⁵³, our results conform with those that report an increment in amplitude and latencies to deviant responses after acute ketamine treatment in rats⁵⁴ and with a sub-anesthetic dose of ketamine in healthy humans producing larger N100 to deviant tones but not MMN⁵⁵. Interestingly, a dose–response study of the MK-801 effects on MMN-like responses in male rats showed that while a high dose (0.5 mg/kg) reduced late deviance detection (around 55 ms), a medium dose (0.3 mg/kg) significantly enhanced early deviance detection effects (at about 13 ms) and some evidence of enhanced late effects although not significantly²². We used a single dose of 0.1 mg/kg in female rats, as it has been demonstrated that females are more sensitive to MK-801 than males³⁴ and that this dose is sufficient to induce behavioral effects⁵⁶. Importantly, memantine, a low-affinity uncompetitive agonist of NMDA-R, has been shown to (i) increase the duration of rodent MMN-like responses³⁰, (ii) increase MMN amplitude in healthy individuals⁵⁷, and (iii) in persons with schizophrenia⁵⁸.

The memantine results suggest an interpretation of our findings in terms of the mechanisms underpinning synaptic plasticity⁵⁹. Partial blockade of NMDA-R (such as mediated by memantine, or low dose MK-801) is also likely to reduce background calcium flux resulting in homeostatic upregulation of NR2B-containing NMDA-Rs leading in turn to the conversion of synapses to a plastic state. That is, while these drugs reduce calcium influx during uncorrelated activity, there is increased calcium influx during correlated activity (produced by physiological stimuli), improved signal to noise, facilitated transmission and increased plasticity^{60–62}.

Different excitatory/inhibitory networks may explain different MK-801 effects along the thalamocortical axis. The increased repetition suppression we observed in the medial geniculate body could also be by altered excitatory/inhibitory balance. Although the rat MGB lacks GABAergic neurons, it receives GABAergic input from the thalamic reticular nucleus (TRN) and the inferior colliculus⁶³. The latter is a source of bottom-up inhibitory influences, while the TRN provides the MGB with an indirect and inhibitory feedback activation from auditory cortex⁶⁴. Cortical stimulation hyperpolarizes TRN neurons and increases their inhibitory output to the MGB⁶⁵ and furthermore, TRN has been demonstrated to profoundly influence SSA in the MGB⁶⁶. Changes in the neuronal firing pattern of thalamic neurons into bursts have been suggested to provide an alerting signal to the somatosensory cortex to enhance stimulus detection⁶⁷. The previous statement supports the idea that following MK-801 treatment we observed a decrement of responses to standard tones,

which could result in a reduced responsiveness of standards. As a consequence, MK-801 would enhance the detection rate of a novel stimulus, a deviant (i.e., increased signal to noise). Overall our results match the general concept that when the system is adapted, it is more sensitive to detect changes in the environment⁶⁸, where a stronger thalamic repetition suppression (or inhibition) supports the increase in the prediction error signals (excitatory) at cortical level or viceversa. It would be interesting to test whether thalamic repetition suppression is correlated with cortical prediction error signals, but this question awaits future experiments.

Other characteristics of the neuronal mechanisms and microcircuitry involving the glutamate NMDA-R system is that NMDA-R are located not only at postsynaptic and presynaptic sites in excitatory neurons, but they are also found at GABAergic inhibitory interneurons in the neocortex⁶⁹. MK-801 has demonstrated a preferential regulation of the firing rate of cortical GABA interneurons, increasing the firing rate of the majority of pyramidal neurons⁷⁰ and therefore producing an imbalance in the excitatory/inhibitory networks in the cortices^{71, 72}. It is well known that cortical GABAergic interneurons differentially amplify stimulus-specific adaptation (a similar phenomenon to iMM) in excitatory pyramidal neurons in the auditory cortex⁷³. Moreover, a model of a mutually coupled excitatory/inhibitory network can explain distinct mechanisms that allow cortical inhibitory neurons to enhance the brain's sensitivity to deviant or unexpected sounds⁷⁴. Further, MK-801 would alter the tonic inhibitory control of NMDA-R in auditory cortical areas leading to the activation of pyramidal neurons by subsequent deviant tones. Thus, the increase in prediction error could arise due to the reciprocal interaction between fast-spiking parvalbumin-positive interneurons and pyramidal neurons. As such, NMDA-R hypofunction of either of these cell types could disturb the excitatory/inhibitory balance that in turn result in the increased or decreased firing of the recorded neurons.

Paradoxical effects of low doses and administration mode of MK-801. Our data are at odds with two previous studies^{17, 75} using similar recording approaches both of which report reduction in deviant responses with NMDA-R antagonist with no effect on neural responses to standards. The reasons for this discrepancy are unclear, but differences in animal species (rats vs. macaques), in the NMDA-R antagonist used (MK-801 vs. ketamine), in drug administration routes (i.p., intramuscular, or local), and/or a combination of these factors may have affected our results. It should also be noted that paradoxical behavioral effects of low doses of MK-801 have been noted previously⁷⁶ as well as differential effects of low (0.1 mg/kg) vs. high (1.0 mg/kg) MK-801 doses on NMDA-R and neuronal activity in pyramidal neurons vs. interneurons³². It is clear that MK-801 effects on both behavior, mRNA expression and protein of NMDA-R subunits are nonlinear and strongly dose-dependent.

Another explanation for our findings is that MK-801 was administered systemically. Thus, MK-801 would affect not only auditory thalamus and auditory cortex, but likely also other regions such as the prefrontal cortex. Furthermore, it is plausible that NMDA-R blockade will also lead to a reduction in direct top-down excitatory input to pyramidal neurons in the auditory cortex from prefrontal cortex^{77, 78}. As discussed in⁷⁹, MK-801 increases activity of prefrontal cortex axons targeting primary visual cortex, reducing the evoked-activity in V1 to repetitive stimuli, possibly mediated through specific subclasses of inhibitory neurons, such as vasoactive intestinal peptide (VIP) interneurons or somatostatin (SST) interneurons. A similar explanation would be plausible for an intermediate region in-between the auditory thalamus and cortex such as the TRN, which may, in turn, suppress the bottom-up thalamic auditory input to auditory cortex. Both mechanisms likely contribute to the alterations of neuronal mismatch we observed as both auditory cortex and auditory thalamus responses are affected. It will be important in the future to further distinguish between these possibilities by, e.g., optogenetic and electrophysiological techniques, in order to target different neuronal populations and probe the activity of the different interneuron subtypes in this model.

Additionally, it is unclear if the effects we observe in single neurons following systemic administration of the drug would be similar to those following local administration of MK-801. A recent publication summarized the literature on effects of systemic vs. local administration MK-801. For example, systemic MK-801 increased glutamate release in medial prefrontal cortex, while local MK-801 did not⁸⁰. Likewise⁸¹, have shown that LFP recordings in urethane-anesthetized rats differ for systemic and local MK-801 applications. There are many potential consequences of systemic NMDA-R blockade, ranging from the alteration of the inputs to MGB from IC and/or to auditory cortex from prefrontal cortex (see above) to differential effects on pyramidal cells versus interneurons in cortex. The reasons for our choice of systemic administration as outlined in the introduction was to mimic as closely as possible the human research on the effects of NMDA-R antagonists on MMN. However, it is clear that future animal studies will be needed to reconcile the divergence of results between the effects of using systemic administration of the present study and localized injections of previous studies (e.g.,¹⁷).

Admittedly, we have only tackled the functional role of the NMDA-R under a particular experimental manipulation, and we cannot exclude the possibility that higher doses of MK-801 would have generated different results. It is also well known that other neuromodulatory systems such as the dopaminergic, cholinergic and/or cannabinoid systems may be altered and interact with the NMDA-Rs in healthy brain function⁸²⁻⁸⁴ as well as in schizophrenia^{71, 85-87}.

Our study is valuable because it has revealed the involvement of two fundamental mechanisms, i.e., repetition suppression and prediction error; and two different pathways, lemniscal and non-lemniscal, underlying the neuronal mismatch in the thalamocortical hierarchy. Predictive coding theory proposes that the brain constantly tries to minimize the discrepancy between actual sensory input and internal representations of the environment⁵. What is new in our data is the critical importance of the hierarchical organization of the auditory system in sharing the 'responsibility' for generating the representation and detecting the discrepancy, mainly attributable to thalamic and cortical processes. However, our data provide evidence that the NMDA-synaptic plasticity and MMN relationship is not as simple as previously surmised from human studies.

MMN and schizophrenia. What are the implications of our findings for schizophrenia given the somewhat unexpected outcome? Reduced MMN is associated with poor global functioning⁸⁸ and cognitive deficits⁸⁹ in schizophrenia. Hence, if a safe drug were available that targeted the relevant NMDA-R subunit, and facilitated neuroplasticity as indexed by increased MMN, it offers opportunities for interventions to remediate cognitive deficits that are a core feature of schizophrenia⁹⁰. Memantine, which has been shown to increase MMN amplitude in healthy individuals and schizophrenia, has been used as adjunctive therapy in schizophrenia for some time to improve cognition in particular. While the effects of adjunctive therapy are small, a recent meta-analysis suggests that there are improvements in global measures of cognition, but enhancements in more sensitive composite cognitive test scores have not been observed⁹¹. To date, there have been no attempts to utilize MMN enhancement to memantine as an index of increased neuroplasticity that could be exploited in remediation studies (but see ⁹² for a suggested galantamine-memantine combination therapy for enhancing MMN, improving cognition and preventing transition to psychosis in a high risk group). Interestingly, both the moderate affinity antagonist, memantine, and high-affinity antagonist, MK-801, bind to the NR2B subunit of the NMDA-R at very similar binding locations⁹³ but only memantine has been approved for use in humans given evidence of neurotoxic effects of MK-801 in humans⁹⁴. One avenue of future research is the development of safe compounds for human use that target similar binding locations to memantine and MK-801.

Data availability

The data that support the findings of this study are available from the corresponding author upon reasonable request.

Received: 16 April 2020; Accepted: 2 July 2020

Published online: 24 July 2020

References

- Näätänen, R., Gaillard, A. W. K. & Mäntysalo, S. Early selective-attention effect on evoked potential reinterpreted. *Acta Psychol.* **42**, 313–329. [https://doi.org/10.1016/0001-6918\(78\)90006-9](https://doi.org/10.1016/0001-6918(78)90006-9) (1978).
- Näätänen, R. & Alho, K. Mismatch negativity—a unique measure of sensory processing in audition. *Int. J. Neurosci.* **80**, 317–337. <https://doi.org/10.3109/00207459508986107> (1995).
- Randeniya, R., Oestreich, L. K. L. & Garrido, M. I. Sensory prediction errors in the continuum of psychosis. *Schizophr. Res.* **191**, 109–122. <https://doi.org/10.1016/j.schres.2017.04.019> (2018).
- Carbajal, G. V. & Malmierca, M. S. The neuronal basis of predictive coding along the auditory pathway: From the subcortical roots to cortical deviance detection. *Trends Hear.* **22**, 2331216518784822. <https://doi.org/10.1177/2331216518784822> (2018).
- Friston, K. A theory of cortical responses. *Philos. Trans. R. Soc. B Biol. Soc.* **360**, 815–836. <https://doi.org/10.1098/rstb.2005.1622> (2005).
- Michie, P. T., Malmierca, M. S., Harms, L. & Todd, J. Understanding the neurobiology of MMN and its reduction in schizophrenia. *Biol. Psychol.* **116**, 1–3. <https://doi.org/10.1016/j.biopsycho.2016.02.00> (2016).
- Bendixen, A., Roeber, U. & Schröger, E. Regularity extraction and application in dynamic auditory stimulus sequences. *J. Cogn. Neurosci.* **19**, 1664–1677. <https://doi.org/10.1162/jocn.2007.19.10.1664> (2007).
- Harms, L. *et al.* Mismatch negativity (MMN) in freely-moving rats with several experimental controls. *PLoS ONE* **9**, e110892. <https://doi.org/10.1371/journal.pone.0110892> (2014).
- Kurkela, J. L. O., Lipponen, A., Kyläheiko, I. & Astikainen, P. Electrophysiological evidence of memory-based detection of auditory regularity violations in anesthetized mice. *Sci. Rep.* **8**, 3027. <https://doi.org/10.1038/s41598-018-21411-z> (2018).
- Nakamura, T. *et al.* Epidural auditory event-related potentials in the rat to frequency and duration deviants: Evidence of mismatch negativity?. *Front. Psychol.* **2**, 367. <https://doi.org/10.3389/fpsyg.2011.00367> (2011).
- Parras, G. G. *et al.* Neurons along the auditory pathway exhibit a hierarchical organization of prediction error. *Nat. Commun.* **8**, 2148. <https://doi.org/10.1038/s41467-017-02038-6> (2017).
- Ishihita, Y. *et al.* Deviance detection is the dominant component of auditory contextual processing in the lateral superior temporal gyrus: A human ECoG study. *Hum. Brain Mapp.* **40**, 1184–1194. <https://doi.org/10.1002/hbm.24438> (2018).
- Umbricht, D. *et al.* Ketamine-induced deficits in auditory and visual context-dependent processing in healthy volunteers: Implications for models of cognitive deficits in schizophrenia. *Arch. Gen. Psychiatry* **57**, 1139–1147. <https://doi.org/10.1001/archpsyc.57.12.1139> (2000).
- Todd, J., Harms, L., Schall, U. & Michie, P. T. Mismatch negativity: Translating the potential. *Front. Psychiatry* **4**, 171. <https://doi.org/10.3389/fpsyg.2013.00171> (2013).
- Umbricht, D., Koller, R., Vollenweider, F. X. & Schmid, L. Mismatch negativity predicts psychotic experiences induced by nmda receptor antagonist in healthy volunteers. *Biol. Psychiatry* **51**, 400–406. [https://doi.org/10.1016/S0006-3223\(01\)01242-2](https://doi.org/10.1016/S0006-3223(01)01242-2) (2002).
- Krystal, J. H. *et al.* Comparative and interactive human psychopharmacologic effects of ketamine and amphetamine. *Arch. Gen. Psychiatry* **62**, 985. <https://doi.org/10.1001/archpsyc.62.9.985> (2005).
- Javitt, D. C., Steinschneider, M., Schroeder, C. E. & Arezzo, J. C. Role of cortical N-methyl-D-aspartate receptors in auditory sensory memory and mismatch negativity generation: Implications for schizophrenia. *Proc. Natl. Acad. Sci.* **93**, 11962–11967. <https://doi.org/10.1073/pnas.93.21.11962> (1996).
- Featherstone, R. E., Melnychenko, O. & Siegel, S. J. Mismatch negativity in preclinical models of schizophrenia. *Schizophr. Res.* **191**, 35–42. <https://doi.org/10.1016/j.schres.2017.07.039> (2018).
- Harms, L. Mismatch responses and deviance detection in N-methyl-D-aspartate (NMDA) receptor hypofunction and developmental models of schizophrenia. *Biol. Psychol.* **116**, 75–81. <https://doi.org/10.1016/j.biopsycho.2015.06.015> (2016).
- Siegel, S. J., Talpos, J. C. & Geyer, M. A. Animal models and measures of perceptual processing in schizophrenia. *Neurosci. Biobehav. Rev.* **37**, 2092–2098. <https://doi.org/10.1016/j.neubiorev.2013.06.016> (2013).
- Tikhonravov, D. *et al.* Effects of an NMDA-receptor antagonist MK-801 on an MMN-like response recorded in anesthetized rats. *Brain Res.* **1203**, 97–102. <https://doi.org/10.1016/j.brainres.2008.02.006> (2008).
- Harms, L. *et al.* Late deviance detection in rats is reduced, while early deviance detection is augmented by the NMDA receptor antagonist MK-801. *Schizophr. Res.* **191**, 43–50. <https://doi.org/10.1016/j.schres.2017.03.042> (2018).
- Traynelis, S. F. *et al.* Glutamate receptor ion channels: Structure, regulation, and function. *Pharmacol. Rev.* **62**, 405–496. <https://doi.org/10.1124/pr.109.002451> (2010).
- Thompson, L. T. & Disterhoft, J. F. N-methyl-D-aspartate receptors in associative eyeblink conditioning: Both MK-801 and phenylclidine produce task- and dose-dependent impairments. *J. Pharmacol. Exp. Ther.* **281**, 928–940 (1997).

25. Takatsuki, K., Kawahara, S., Takehara, K., Kishimoto, Y. & Kirino, Y. Effects of the noncompetitive NMDA receptor antagonist MK-801 on classical eyeblink conditioning in mice. *Neuropharmacology* **41**, 618–628. [https://doi.org/10.1016/S0028-3908\(01\)00113-7](https://doi.org/10.1016/S0028-3908(01)00113-7) (2001).
26. Rodríguez-Moreno, A., Carrión, M. & Delgado-García, J. M. The nicotinic agonist RJR-2403 compensates the impairment of eyeblink conditioning produced by the noncompetitive NMDA-receptor antagonist MK-801. *Neurosci. Lett.* **402**, 102–107. <https://doi.org/10.1016/j.neulet.2006.03.053> (2006).
27. Harms, L., Parras, G. G., Michie, P. T. & Malmierca, M. S. The role of glutamate neurotransmission in mismatch negativity (MMN), a measure of auditory synaptic plasticity and change-detection. *Neuroscience* <https://doi.org/10.1016/j.neuroscience.2020.01.046> (2020).
28. Ehrlichman, R. S., Maxwell, C. R., Majumdar, S. & Siegel, S. J. Deviance-elicited changes in event-related potentials are attenuated by ketamine in mice. *J. Cogn. Neurosci.* **20**, 1403–1414. <https://doi.org/10.1162/jocn.2008.20097> (2008).
29. Sivarao, D. V. *et al.* NR2B antagonist CP-101,606 abolishes pitch-mediated deviance detection in awake rats. *Front. Psychiatry* **5**, 96. <https://doi.org/10.3389/fpsy.2014.00096> (2014).
30. Tikhonravov, D. *et al.* Dose-related effects of memantine on a mismatch negativity-like response in anesthetized rats. *Neuroscience* **167**, 1175–1182. <https://doi.org/10.1016/j.neuroscience.2010.03.014> (2010).
31. Duque, D., Ayala, Y. A. & Malmierca, M. S. Deviance detection in auditory subcortical structures: What can we learn from neurochemistry and neural connectivity?. *Cell Tissue Res.* **361**, 215–232. <https://doi.org/10.1007/s00441-015-2134-7> (2015).
32. Xi, D., Zhang, W., Wang, H.-X., Stradtman, G. G. & Gao, W.-J. Dizocilpine (MK-801) induces distinct changes of N-methyl-D-aspartic acid receptor subunits in parvalbumin-containing interneurons in young adult rat prefrontal cortex. *Int. J. Neuropsychopharmacol.* **12**, 1395. <https://doi.org/10.1017/S146114570900042X> (2009).
33. Hönack, D. & Löscher, W. Sex differences in NMDA receptor mediated responses in rats. *Brain Res.* **620**, 167–170. [https://doi.org/10.1016/0006-8993\(93\)90287-W](https://doi.org/10.1016/0006-8993(93)90287-W) (1993).
34. Andine, P. *et al.* Characterization of MK-801-induced behavior as a putative rat model of psychosis. *J. Pharmacol. Exp. Ther.* **290**, 1393–1408. <https://doi.org/10.1088/0741-3335/49/12B/S19> (1999).
35. Opitz, B., Schröger, E. & Von Cramon, D. Y. Sensory and cognitive mechanisms for preattentive change detection in auditory cortex. *Eur. J. Neurosci.* **21**, 531–535. <https://doi.org/10.1111/j.1460-9568.2005.03839.x> (2005).
36. Ruhnau, P., Herrmann, B. & Schröger, E. Clinical Neurophysiology Finding the right control: The mismatch negativity under investigation. *Clin. Neurophysiol.* **123**, 507–512. <https://doi.org/10.1016/j.clinph.2011.07.035> (2012).
37. Duque, D. & Malmierca, M. S. Stimulus-specific adaptation in the inferior colliculus of the mouse: Anesthesia and spontaneous activity effects. *Brain Struct. Funct.* **220**, 3385–3398. <https://doi.org/10.1007/s00429-014-0862-1> (2015).
38. Pérez-González, D., Hernández, O., Covey, E. & Malmierca, M. S. GABAA-mediated inhibition modulates stimulus-specific adaptation in the inferior colliculus. *PLoS ONE* **7**, e34297. <https://doi.org/10.1371/journal.pone.0034297> (2012).
39. Duque, D., Pais, R. & Malmierca, M. S. Stimulus-specific adaptation in the anesthetized mouse revealed by brainstem auditory evoked potentials. *Hear. Res.* **370**, 294–301. <https://doi.org/10.1016/j.heares.2018.08.011> (2018).
40. Antunes, F. M., Nelken, I., Covey, E. & Malmierca, M. S. Stimulus-specific adaptation in the auditory thalamus of the anesthetized rat. *PLoS ONE* **5**, e14071. <https://doi.org/10.1371/journal.pone.0014071> (2010).
41. Nieto-Diego, J. & Malmierca, M. S. Topographic distribution of stimulus-specific adaptation across auditory cortical fields in the anesthetized rat. *PLOS Biol.* **14**, e1002397. <https://doi.org/10.1371/journal.pbio.1002397> (2016).
42. Vezzani, A. *et al.* Kinetics of MK-801 and its effect on quinolinic acid-induced seizures and neurotoxicity in rats. *J. Pharmacol. Exp. Ther.* **249**, 278–283 (1989).
43. Paxinos, G. & Watson, C. *The Rat Brain in Stereotaxic Coordinates*: Hard Cover Edition. 466 (2013). ISBN: 9780124157521
44. Pérez-González, D. & Malmierca, M. S. Variability of the time course of stimulus-specific adaptation in the inferior colliculus. *Front. Neural Circuits* <https://doi.org/10.3389/fncir.2012.00107> (2012).
45. Wiens, S., Szychowska, M., Eklund, R. & van Berlekom, E. Cascade and no-repetition rules are comparable controls for the auditory frequency mismatch negativity in oddball tasks. *Psychophysiology* **56**, e13280. <https://doi.org/10.1111/psyp.13280> (2019).
46. Hu, B. Functional organization of lemniscal and nonlemniscal auditory thalamus. *Exp. Brain Res.* **153**, 543–549. <https://doi.org/10.1007/s00221-003-1611-5> (2003).
47. Lee, C. & Sherman, S. M. On the classification of pathways in the auditory midbrain, thalamus, and cortex. *Hear. Res.* **276**, 79–87. <https://doi.org/10.1016/j.heares.2010.12.012> (2011).
48. Antunes, F. M. & Malmierca, M. S. An overview of stimulus-specific adaptation in the auditory thalamus. *Brain Topogr.* **27**, 480–499. <https://doi.org/10.1007/s10548-013-0342-6> (2014).
49. Blanke, M. L. & VanDongen, A. M. J. Activation Mechanisms of the NMDA Receptor (Chapter 13). *Biology of the NMDA Receptor* (CRC Press/Taylor & Francis, 2009). ISBN: 9781420044140
50. Wacongne, C. A predictive coding account of MMN reduction in schizophrenia. *Biol. Psychol.* **116**, 68–74. <https://doi.org/10.1016/j.biopsycho.2015.10.011> (2016).
51. Aukstulewicz, R. & Friston, K. Repetition suppression and its contextual determinants in predictive coding. *Cortex.* **80**, 125–140. <https://doi.org/10.1016/j.cortex.2015.11.024> (2016).
52. Voss, P., Thomas, M. E., Guercio, G. D. & de Villers-Sidani, E. Dysregulation of auditory neuroplasticity in schizophrenia. *Schizophr. Res.* **207**, 3–11. <https://doi.org/10.1016/j.schres.2018.04.025> (2019).
53. Schuelert, N., Dorner-Ciossek, C., Brendel, M. & Rosenbrock, H. A comprehensive analysis of auditory event-related potentials and network oscillations in an NMDA receptor antagonist mouse model using a novel wireless recording technology. *Physiol. Rep.* **6**, e13782. <https://doi.org/10.14814/phy2.13782> (2018).
54. Ahnaou, A., Huysmans, H., Biermans, R., Manyakov, N. V. & Drinkenburg, W. H. I. M. Ketamine: Differential neurophysiological dynamics in functional networks in the rat brain. *Transl. Psychiatry* **7**, e1237–e1237. <https://doi.org/10.1038/tp.2017.198> (2017).
55. Oranje, B. The effects of a sub-anesthetic dose of ketamine on human selective attention. *Neuropsychopharmacology* **22**, 293–302. [https://doi.org/10.1016/S0893-133X\(99\)00118-9](https://doi.org/10.1016/S0893-133X(99)00118-9) (2000).
56. Meehan, C. *et al.* Effects of immune activation during early or late gestation on schizophrenia-related behaviour in adult rat offspring. *Brain. Behav. Immun.* **63**, 8–20. <https://doi.org/10.1016/j.bbi.2016.07.144> (2017).
57. Korostenskaja, M., Nikulin, V. V., Kičić, D., Nikulina, A. V. & Kähkönen, S. Effects of NMDA receptor antagonist memantine on mismatch negativity. *Brain Res. Bull.* **72**, 275–283. <https://doi.org/10.1016/j.brainresbull.2007.01.007> (2007).
58. Swerdlow, N. R. *et al.* Memantine effects on sensorimotor gating and mismatch negativity in patients with chronic psychosis. *Neuropsychopharmacology* **41**, 419–430. <https://doi.org/10.1038/npp.2015.162> (2016).
59. Slutsky, I., Sadeghpour, S., Li, B. & Liu, G. Enhancement of synaptic plasticity through chronically reduced Ca²⁺ flux during uncorrelated activity. *Neuron* **44**, 835–849. <https://doi.org/10.1016/j.neuron.2004.11.013> (2004).
60. Slutsky, I. *et al.* Enhancement of learning and memory by elevating brain magnesium. *Neuron* **65**, 165–177. <https://doi.org/10.1016/j.neuron.2009.12.026> (2010).
61. de Sevilla, D. F. & Buno, W. The muscarinic long-term enhancement of NMDA and AMPA receptor-mediated transmission at Schaffer collateral synapses develop through different intracellular mechanisms. *J. Neurosci.* **30**, 11032–11042. <https://doi.org/10.1523/JNEUROSCI.1848-10.2010> (2010).
62. Nuñez, A., Domínguez, S., Buño, W. & de Sevilla, D. F. Cholinergic-mediated response enhancement in barrel cortex layer V pyramidal neurons. *J. Neurophysiol.* **108**, 1656–1668. <https://doi.org/10.1152/jn.00156.2012> (2012).

63. Malmierca, M. S. Auditory System (Chapter 29). In *The Rat Nervous System* (ed Paxinos, G.) 865–946 (Academic Press, Cambridge). <https://doi.org/10.1016/B978-0-12-374245-2.00029-2> (2015).
64. Bartlett, E. L. The organization and physiology of the auditory thalamus and its role in processing acoustic features important for speech perception. *Brain Lang.* **126**, 29–48. <https://doi.org/10.1016/j.bandl.2013.03.003> (2013).
65. Crabtree, J. W., Lodge, D., Bashir, Z. I. & Isaac, J. T. R. GABA_A, NMDA and mGlu2 receptors tonically regulate inhibition and excitation in the thalamic reticular nucleus. *Eur. J. Neurosci.* **37**, 850–859. <https://doi.org/10.1111/ejn.12098> (2013).
66. Yu, X.-J., Xu, X.-X., He, S. & He, J. Change detection by thalamic reticular neurons. *Nat. Neurosci.* **12**, 1165–1170. <https://doi.org/10.1038/nn.2373> (2009).
67. Hu, H. & Agmon, A. Differential excitation of distally versus proximally targeting cortical interneurons by unitary thalamocortical bursts. *J. Neurosci.* **36**, 6906–6916. <https://doi.org/10.1523/JNEUROSCI.0739-16.2016> (2016).
68. Musall, S. *et al.* Tactile frequency discrimination is enhanced by circumventing neocortical adaptation. *Nat. Neurosci.* **17**, 1567–1573. <https://doi.org/10.1038/nn.3821> (2014).
69. DeBiasi, S., Minelli, A., Melone, M. & Conti, F. Presynaptic NMDA receptors in the neocortex are both auto- and heteroreceptors. *NeuroReport* **7**, 2773–2776. <https://doi.org/10.1097/00001756-199611040-00073> (1996).
70. Homayoun, H. & Moghaddam, B. NMDA receptor hypofunction produces opposite effects on prefrontal cortex interneurons and pyramidal neurons. *J. Neurosci.* **27**, 11496–11500. <https://doi.org/10.1523/JNEUROSCI.2213-07.2007> (2007).
71. Okada, M., Fukuyama, K., Kawano, Y., Shiroyama, T. & Ueda, Y. Memantine protects thalamocortical hyper-glutamatergic transmission induced by NMDA receptor antagonism via activation of system xc⁻. *Pharmacol. Res. Perspect.* **7**, e00457. <https://doi.org/10.1002/prp2.457> (2019).
72. Bygrave, A. M. *et al.* Knockout of NMDA-receptors from parvalbumin interneurons sensitizes to schizophrenia-related deficits induced by MK-801. *Transl. Psychiatry* **6**, e778. <https://doi.org/10.1038/tp.2016.44> (2016).
73. Chen, I.-W., Helmchen, F. & Lutcke, H. Specific early and late oddball-evoked responses in excitatory and inhibitory neurons of mouse auditory cortex. *J. Neurosci.* **35**, 12560–12573. <https://doi.org/10.1523/JNEUROSCI.2240-15.2015> (2015).
74. Natan, R. G. *et al.* Complementary control of sensory adaptation by two types of cortical interneurons. *Elife* <https://doi.org/10.7554/eLife.09868> (2015).
75. Lakatos, P. *et al.* The thalamocortical circuit of auditory mismatch negativity. *Biol. Psychiatry* <https://doi.org/10.1016/j.biopsych.2019.10.029> (2019).
76. Tang, Y. *et al.* Paradoxical effects of very low dose MK-801. *Eur. J. Pharmacol.* **537**, 77–84. <https://doi.org/10.1016/j.ejphar.2006.03.016> (2006).
77. Rosch, R. E., Auksztulewicz, R., Leung, P. D., Friston, K. J. & Baldeweg, T. Selective prefrontal disinhibition in a roving auditory oddball paradigm under N-methyl-D-aspartate receptor blockade. *Biol. Psychiatry Cogn. Neurosci. Neuroimaging* **4**, 140–150. <https://doi.org/10.1016/j.bpsc.2018.07.003> (2019).
78. Schmidt, A. *et al.* Modeling ketamine effects on synaptic plasticity during the mismatch negativity. *Cereb. Cortex* **23**, 2394–2406. <https://doi.org/10.1093/cercor/bhs238> (2013).
79. Ranson, A. *et al.* Top-down suppression of sensory cortex in an NMDAR hypofunction model of psychosis. *Schizophr. Bull.* **45**, 1349–1357. <https://doi.org/10.1093/schbul/sby190> (2019).
80. Fukuyama, K., Kato, R., Murata, M., Shiroyama, T. & Okada, M. Clozapine normalizes a glutamatergic transmission abnormality induced by an impaired NMDA receptor in the thalamocortical pathway via the activation of a group III metabotropic glutamate receptor. *Biomolecules* **9**, 234. <https://doi.org/10.3390/biom9060234> (2019).
81. Kiss, T. *et al.* Role of thalamic projection in NMDA receptor-induced disruption of cortical slow oscillation and short-term plasticity. *Front. Psychiatry* **2**, 1–12. <https://doi.org/10.3389/fpsy.2011.00014> (2011).
82. Ayala, Y. A., Pérez-González, D. & Malmierca, M. S. Stimulus-specific adaptation in the inferior colliculus: The role of excitatory, inhibitory and modulatory inputs. *Biol. Psychol.* **116**, 10–22. <https://doi.org/10.1016/j.biopsycho.2015.06.016> (2016).
83. Valdés-Baizabal, C., Parras, G. G., Ayala, Y. A. & Malmierca, M. S. Endocannabinoid modulation of stimulus-specific adaptation in inferior colliculus neurons of the rat. *Sci. Rep.* **7**, 6997. <https://doi.org/10.1038/s41598-017-07460-w> (2017).
84. Valdés-Baizabal, C., Carbajal, G. V., Pérez-González, D. & Malmierca, M. S. Dopamine modulates subcortical responses to surprising sounds. *PLoS Biol.* **18**(6), e3000744. <https://doi.org/10.1371/journal.pbio.3000744> (2020).
85. Howes, O. H. & Kaar, S. J. Antipsychotic drugs: Challenges and future directions. *World Psychiatry* **17**, 170–171. <https://doi.org/10.1002/wps.20522> (2018).
86. Lucatch, A. M., Coles, A. S., Hill, K. P. & George, T. P. Cannabis and Mood disorders. *Curr. Addict. Rep.* **5**, 336–345. <https://doi.org/10.1007/s40429-018-0214-y> (2018).
87. Parr, T. & Friston, K. J. The anatomy of inference: Generative models and brain structure. *Front. Comput. Neurosci.* **12**, 90. <https://doi.org/10.3389/fncom.2018.00090> (2018).
88. Light, G. A. & Braff, D. L. Mismatch negativity deficits are associated with poor functioning in schizophrenia patients. *Arch. Gen. Psychiatry* **62**, 127. <https://doi.org/10.1001/archpsyc.62.2.127> (2005).
89. Baldeweg, T., Klugman, A., Gruzelier, J. & Hirsch, S. R. Mismatch negativity potentials and cognitive impairment in schizophrenia. *Schizophr. Res.* **69**, 203–217. <https://doi.org/10.1016/j.schres.2003.09.009> (2004).
90. Green, M. F., Kern, R. S., Braff, D. L. & Mintz, J. Neurocognitive deficits and functional outcome in schizophrenia: Are we measuring the ‘right stuff’?. *Schizophr. Bull.* **26**, 119–136. <https://doi.org/10.1093/oxfordjournals.schbul.a033430> (2000).
91. Kishi, T. *et al.* Anti-dementia drugs for psychopathology and cognitive impairment in schizophrenia: A systematic review and meta-analysis. *Int. J. Neuropsychopharmacol.* **21**, 748–757. <https://doi.org/10.1093/ijnp/pyy045> (2018).
92. Koola, M. M. Attenuated mismatch negativity in attenuated psychosis syndrome predicts psychosis: Can galantamine-memantine combination prevent psychosis?. *Mol. Neuropsychiatry* **4**, 71–74. <https://doi.org/10.1159/000488797> (2018).
93. Song, X. *et al.* Mechanism of NMDA receptor channel block by MK-801 and memantine. *Nature* **556**, 515–519. <https://doi.org/10.1038/s41586-018-0039-9> (2018).
94. Olney, J., Labruyere, J. & Price, M. Pathological changes induced in cerebrotal neurons by phencyclidine and related drugs. *Science* **244**, 1360–1362. <https://doi.org/10.1126/science.2660263> (1989).

Acknowledgements

We thank Drs. Javier Nieto-Diego and David Perez-Gonzalez for their technical support and constructive criticisms; and Drs. Nashat Abumaria and Juanita Todd for advice and constructive comments on the discussion. We also thank Dr. Marianny Janiree Pernía Rosales for helping with the histological photomicrography and Mr. Antonio Rivas Cornejo for the technical support. This work was supported by the Spanish MINECO (SAF2016-75803-P) and JCYL (SA023P17) to MSM. GGP held a fellowship from the Spanish MINECO (BES-2014-069113), and CVB held a fellowship from Mexican CONACyT (216652). LH was supported by an NHMRC project grant: APP1109283.

Author contributions

G.G.P.: conceptualization, investigation, formal analysis, writing—original draft; C.V.B.: investigation; LH: conceptualization, writing—review and editing; P.T.M.: conceptualization, writing—review and editing; M.S.M.: conceptualization, writing—review and editing, supervision, project administration, funding acquisition.

Competing interests

The authors declare no competing interests.

Additional information

Correspondence and requests for materials should be addressed to M.S.M.

Reprints and permissions information is available at www.nature.com/reprints.

Publisher's note Springer Nature remains neutral with regard to jurisdictional claims in published maps and institutional affiliations.



Open Access This article is licensed under a Creative Commons Attribution 4.0 International License, which permits use, sharing, adaptation, distribution and reproduction in any medium or format, as long as you give appropriate credit to the original author(s) and the source, provide a link to the Creative Commons license, and indicate if changes were made. The images or other third party material in this article are included in the article's Creative Commons license, unless indicated otherwise in a credit line to the material. If material is not included in the article's Creative Commons license and your intended use is not permitted by statutory regulation or exceeds the permitted use, you will need to obtain permission directly from the copyright holder. To view a copy of this license, visit <http://creativecommons.org/licenses/by/4.0/>.

© The Author(s) 2020